International Journal of Concrete Structures and Materials

REVIEW

Open Access

Ultra-High-Strength Lightweight Fiber-Reinforced Concrete: A Review

Su Sung Jo[1], Tan Duy Phan[2], Do Hyung Lee[3], Sang Yeop Chung[4] and Dong Joo Kim[2*]

Abstract

This study provides a comprehensive overview of the material and mechanical properties of lightweight fiber-reinforced cementitious composites (L-FRCCs), focusing on their classification as ultra-high-strength lightweight fiber-reinforced cementitious composites (UL-FRCCs). The L-FRCCs exhibit a density of 1440–2150 kg/m^3, thermal coefficient of 0.22–0.33 W/mK, compressive strength of 45–145 MPa, and flexural strength of 4.3–37.5 MPa. The strength of the L-FRCCs increases linearly with matrix strength. Specifically, L-FRCCs with compressive strength > 100 MPa, flexural strength < 15 MPa, density < 1950 kg/m^3, and thermal conductivity < 0.5 W/mK can be classified as UL-FRCCs. Pearson correlation analysis reveals that the structural efficiency (SE) of L-FRCCs increases with increasing matrix strength, fiber volume content, and reinforcing index; however, it decreases with an increase in the lightweight aggregate (LWA) ratio. For UL-FRCCs to achieve optimal SE, the LWAs should possess a crushing strength > 70 MPa and specific gravity < 0.5. Additionally, incorporating straight steel fibers at volumes < 2.5% is recommended to achieve strengths > 100 MPa. Compared to nonmetallic fibers such as polymeric fibers, steel fibers offer superior SE for flexural strength, despite their tendency to reduce workability owing to their high stiffness.

Keywords Lightweight fiber-reinforced cementitious composites, Ultra-high-strength lightweight fiber-reinforced cementitious composites, Structural efficiency, Fiber, Lightweight aggregate

1 Introduction

Conventional concrete prepared with normal-weight aggregates is a widely used primary material in the field of civil engineering; however, it has some significant drawbacks, such as high density and relatively high thermal conductivity. To improve the overall performance of concrete structures, advanced materials such as lightweight concrete (LWC), high-strength concrete, ultra-high-strength concrete, and ultra-high-performance concrete (UHPC) have been developed. BS EN 1992-1-1 (Design of Concrete Structures) defines LWC as concrete with an oven-dry density of less than 2200 kg/m^3 (EN, 2004), and ASTM C1856 specifies that UHPC must achieve a minimum compressive strength of 120 MPa (ASTMC, 2017). The type and proportion of lightweight aggregates (LWAs) used in LWC strongly influence its mechanical properties. Therefore, the performance of LWC is commonly evaluated based on both compressive strength and density. This has led to the development of lightweight fiber-reinforced cementitious composites (L-FRCCs), which exhibit reduced self-weight, high strength, improved thermal insulation, and lower construction costs. Compared to LWC, normal concrete, and fiber-reinforced cementitious composites, L-FRCCs typically exhibit lower thermal conductivity, increased ion penetration, higher fire resistance, and higher sound

Journal information: ISSN 1976-0485/eISSN 2234-1315

*Correspondence:
Dong Joo Kim
djkim75@hanyang.ac.kr
[1] Department of Civil and Environmental Engineering, Sejong University, 209, Neungdong-Ro, Gwangjin-Gu, Seoul 05006, Republic of Korea
[2] Department of Civil and Environmental Engineering, Hanyang University, 222 Wangsimni-Ro, Seongdong-Gu, Seoul 04763, Republic of Korea
[3] Department of Civil, Raiload and Unmanned Systems Engineering, PaiChai University, Daejeon 35345, Republic of Korea
[4] Department of Civil and Environmental Engineering, Yonsei University, Seoul 03722, Republic of Korea

absorption capabilities (Abid et al., 2024; Alanazi et al., 2022; Balendran et al., 2002; Dawood & Hamad, 2013; Guo et al., 2023; Jiang et al., 2024; Li et al., 2016, 2025; Lu et al., 2022a; Meng et al., 2023; Shen et al., 2020a; Shi et al., 2024; Wang & Wang, 2013; Wu et al., 2021; Xie et al., 2022; Yu et al., 2021; Zhang et al., 2024, 2025; Zheng et al., 2025). With recent developments in reactive powder concrete (RPC) and UHPC, the load-bearing capacity and durability have significantly improved. Moreover, the use of hollow glass microspheres (HGMs)—a novel LWA—has notably reduced the density of L-FRCCs with minimal loss of strength (Dahal et al., 2022; Dawood & Hamad, 2013; Guo et al., 2023; Lu et al., 2021a, 2022b; Zhang et al., 2025).

L-FRCCs can provide structural engineers and building designers the flexibility to design and construct various structures (Balendran et al., 2002). In particular, ultra-high-strength lightweight fiber-reinforced cementitious composites (UL-FRCCs) incorporating a high volume of HGMs (replacement amount: 25% for cement and 50% for sand by volume) in UHPC have successfully demonstrated very low chloride ion penetration owing to factors such as the densified matrix structure of UHPC, high strength of over 140 MPa, and low density (1862 kg/m^3) (Dahal et al., 2022).

Structural efficiency (SE), defined as the ratio between material strength and density, is a key parameter in developing lightweight and high-performance cementitious composites. The high SE and densified matrix structure of UL-FRCCs is expected to facilitate the development of new types of concrete structures (Balendran et al., 2002; Dawood & Hamad, 2013; Jiang et al., 2024; Liao et al., 2025; Lu et al., 2022b; Mohamed et al., 2023; Wang & Wang, 2013). There have been several efforts toward increasing the SE of L-FRCCs by exploring different binders and LWAs. A higher SE indicates that a material can meet equivalent structural requirements with less weight, which is essential for the practical application of L-FRCCs in the construction industry (Lu, 2023). Several methods have been proposed to develop L-FRCCs with high SE. Combining high-strength cement matrix and LWAs during the production of lightweight cementitious composites can help improve mechanical properties (Li et al., 2016; Liao et al., 2025; Poongodi & Murthi, 2020; Tang, 2020; Xie et al., 2022; Yu et al., 2021). The addition of fibers plays a crucial role in preventing matrix cracking, minimizing the crack opening of the matrix, and enhancing the fracture toughness, tensile strength, and energy absorption capacity (Jiang et al., 2024; Li et al., 2016; Liao et al., 2025; Tang, 2020; Yew et al., 2015; Zhang et al., 2024, 2025). Lu et al. (Lu et al., 2021b) highlighted three essential strategies for fabricating high-performance and high-strength lightweight cementitious composites: (1) utilizing high-quality binder matrices, (2) selecting appropriate LWAs, and (3) employing fiber reinforcement.

Table 1 lists various L-FRCCs with compressive strengths ranging from 45–160 MPa. The table further summarizes the material properties of the L-FRCCs corresponding to different types of LWAs and fibers. According to ACI 213R (2014) (Liu et al., 2021), LWC with a compressive strength > 40 MPa is classified as high-strength structural lightweight concrete. Moreover, ACI 363R defines high-strength concrete as concrete with a compressive strength > 55 MPa (ACI Committee, 2010). In this study, L-FRCCs with a compressive strength > 45 MPa were investigated to propose a suitable strategy for enhancing both SE and mechanical properties of L-FRCCs, and developing UL-FRCCs. Several studies have been conducted on L-FRCCs, as listed in Table 1. Since the late 2010s, many researchers in the USA, Korea, and China have incorporated HGMs and cenospheres in UHPCs to develop UL-FRCCs with densities less than 1950 kg/m^3 and strengths exceeding 100 MPa (Alanazi et al., 2022; Dahal et al., 2022; Guo et al., 2023; Li et al., 2022; Lu et al., 2021a, 2021b, 2022a, 2022b; Meng et al., 2023; Shen et al., 2020a, 2021; Wu et al., 2021; Xie et al., 2022). Numerous LWAs, fibers, and matrices have also been utilized (Table 1). The most widely used LWAs include expanded clay, expanded shale, sintered fly ash, cenospheres, and HGMs. Furthermore, some widely adopted fibers include steel, carbon, glass, polymers, and natural fibers, as summarized in Table 1.

Many studies have applied various types and contents of fibers and LWAs, aiming to increase the SE of L-FRCCs (Abid et al., 2024; ACI Committee, 2010; Altalabani et al., 2020; Arel & Shaikh, 2018; Balendran et al., 2002; Gondokusumo et al., 2021; Güneyisi et al., 2013; Guo et al., 2023; Iqbal et al., 2015; Kayali et al., 2003; Li et al., 2021a, 2022, 2025; Liao et al., 2025; Mailyan et al., 2021; Mo et al., 2014; Trabelsi & Kammoun, 2020; Wang et al., 2013; Wei et al., 2020; Yahaghi et al., 2016; Yap et al., 2016; Ye et al., 2020; Yew et al., 2015; Zhang et al., 2025; Zhao et al., 2016). The use of lightweight materials significantly decreases the density (Gencel et al., 2022; Lu et al., 2021a, 2022b), as it increases the porosity of the matrix, and consequently decreases the mechanical resistance (Guo et al., 2023; Jiang et al., 2024; Lu et al., 2021a; Shi et al., 2024; Xie et al., 2022; Yu et al., 2021; Zheng et al., 2025). Incorporating short fibers in a single or hybrid form to lightweight cementitious composites leads to a significant increase in flexural and tensile strengths compared to normal LWC owing to the fiber bridging effect (Abid et al., 2024; Chen & Liu, 2005; Jiang et al., 2024; Liao et al., 2025; Zhang et al., 2024). Although

Table 1 Summary of previous studies on lightweight fiber-reinforced cementitious composites (L-FRCCs)

Year	Country	Matrix	Fiber	LWA	γ [a]	f_{ck} [b]	f_{MOR} [c]	f_t [d]	κ [e]	Ref
1997	China	LCC[f]	Steel	ECLA[i]	1960	85.4	11.8	8.8	–	Gao et al. (1997)
2002	China	LCC	Steel	SFLA[j]	2030	91.0	11.3	6.2	–	Balendran et al. (2002)
2003	Australia	LCC	Steel	SFLA	2030	91.0	11.3	6.2	–	Kayali et al. (2003)
2010	USA	LCC	PVA[o]	Poly vinyl butyral	1548	–	7.6		–	Xu et al. (2010)
2013	China	LCC	Steel	ESLA[k]	–	74.8	–	7.7	–	Wang et al. (2013)
2013	Singapore	LCC	Steel + PE	FCLA	1468	68.0	6.8	–	–	Wang et al. (2013)
2013	Turkey	LCC	Steel	SFLA	–	46.8	-	4.2	–	Guneyisi et al. (2013)
2014	Malysia	LCC	Steel + PP	OPS[m]	1870	49.4	–	–	–	Mo et al. (2014)
2014	South Korea	LCC	Vinylon	ESLA	1640	46.1	6.0	4.1	-	Choi et al. (2014)
2015	Germany	LCC	Steel	ECLA	1695	64.0	4.4	4.8	-	Iqbal et al. (2015)
2016	China	LCC	PP[p]	SFLA	–	–	–	–	–	Li et al. (2016)
2016	China	LCC	Steel	ESLA	1843	64.8	–	–	–	Zhao et al. (2016)
2016	Malysia	LCC	Steel	OPS	2002	47.3	8.2	–	–	Yap et al. (2016)
2016	Malysia	LCC	PP	OPS	1996	46.3	5.0	3.9	–	Yahaghi et al. (2016)
2018	Turkey	LCC	Steel	OPS	1725	59.0	–	–	–	Arel et al. (2018)
2018	Oman	LCC	PVA	FCLA + ECLA	1440	62.0	6.4	–	–	Sohel et al. (2018)
2018	Portugal	LCC	PP	ECLA	1900	45.1	8.6	–	–	Frazao et al. (2018)
2019	China	LCC	Carbon	ESLA	1845	86.1	5.9	10.0	–	Liu et al. (2019a)
2019	China	LCC	Steel	ESLA	1897	86.1	5.9	10.1	–	Wu et al. (2019)
2019	China	LCC	Steel	ESLA	–	45.0	–	3.3	–	Zheng et al. (2019)
2019	China	U-LCC[g]	Steel	FCLA[h]	2045	105.2	14.8	–	–	Wu et al. (2021)
2020	China	LCC	Basalt	SFLA	–	64.0	5.3	5.0	–	Zeng et al. (2020)
2020	China	LCC	Carbon	ESLA	1844	67.1	6.4	3.7	–	Wei et al. (2020)
2020	China	LCC	Steel	ESLA	1997	81.3	8.5	8.7	–	Ye et al. (2020)
2020	China	ULCC	Steel	ESLA	–	–	–	–	–	Shen et al. (2020a)
2020	Germany	LCC	PP	ECLA	1737	61.3	7.5	4.5	–	Altalabani et al. (2020)
2020	Iraq	LCC	Steel + PP	Bentonite clay	1835	48.5	–	–	–	Hussein et al. (2020)
2020	Taiwan	LCC	PP	Reservoir sludge	2045	52.0	5.0	–	–	Tang et al. (2020)
2020	Tunisia	LCC	Prickly pear	Dune sand	1970	58.2	14.0	–	1.20	Trabelsi et al. (2020)
2021	China	ULCC	Steel	ESLA	2150	85.0	–	–	0.65	Lu et al. (2021b)
2021	China	LCC	Steel	ESLA	1894	63.5	11.5	4.5	–	Li et al. (2021a)
2021	China	ULCC	Steel	Ceramsite sand	2005	118.0	17.5	–	–	Xie et al. (2022)
2021	China	ULCC	Steel	HGM[l]	1825	125.0	20.0	–	–	Lu et al. (2021a)
2021	USA	LCC	PE[n]	Rubber + FCLA	1790	62.0	–	11.3	–	Yu et al. (2021)
2021	Russia	LCC	Basalt	Pumice	1888	66.6	7.9	4.6	–	Mailyan et al. (2021)
2021	Russia	LCC	Glass	Pumice	2095	58.9	16.9	6.2	–	Shcherban et al. (2021)
2021	Singapore	LCC	Steel	ESLA	1919	62.0	10.0	–	–	Gondokusumo et al. (2021)
2021	Australia	LCC	Polyolefin	Stalite	1867	90.2	4.3	5.6	–	Liu et al. (2021)
2022	China	LCC	Steel	SFLA	1907	74.9	–	–	–	Xiang et al. (2022)
2022	China	ULCC	Steel	HGM	1880	115.0	37.5	–	1.2	Lu et al. (2022b)
2022	China	ULCC	Steel	ESLA	1870	126.7	20.1	–	–	Li et al. (2022)
2022	Malysia	LCC	Steel	ECLA	1934	54.1	–	–	1.22	Shafigh et al. (2022)
2022	South Korea	ULCC	Steel	HGM	1862	145.0	–	–	–	Dahal et al. (2022)
2022	Oman	LCC	Steel	OPS	–	61.3	15.2	-	–	Hosen et al. (2022)
2022	Iran	LCC	Steel	ECLA	–	50.2	13.6	4.6	–	Esmaeili et al. (2023)
2022	Saudi Arabia	ULCC	Steel	-	–	113.0	25.0	–	–	Alanazi et al. (2022)
2023	China	ULCC	Steel	SFLA	1994	83.7	17.5	–	–	Meng et al. (2023)
2023	USA	ULCC	PE	HGM + expanded glass	2006	127.0	21.3	–	0.65	Guo et al. (2023)
2024	China	LCC	Steel	SFLA	–	54	–	–	–	Jiang et al. (2024)

Table 1 (continued)

Year	Country	Matrix	Fiber	LWA	γ [a]	f_{ck} [b]	f_{MOR} [c]	f_t [d]	κ [e]	Ref
2024	China	ULCC	Steel	ECLA	2100	132.7	–	–	–	Zhang et al. (2024)
2024	China	ULCC	Basalt	ESLA	1950	85	–	–	–	Shi et al. (2024)
2024	Pakistan	LCC	Basalt	ESLA	1777	51.65	9.39	4.26	–	Abid et al. (2024)
2025	China	LCC	PVA	CCS[q]	–	71.87	–	–	–	Zheng et al. (2025)
2025	Hong Kong	ULCC	Steel	CSLA	1907	81.03	–	6.68	–	Liao et al. (2025)

[a] Density (γ) [kg/m^3]

[b] Compressive strength (f_{ck}) [MPa]

[c] Flexural strength at modulus of rupture (f_{MOR}) [MPa]

[d] Tensile strength (f_t) [MPa]

[e] Thermal conductivity (κ) [W/mk]

[f] Lightweight cementitious composite

[g] Ultra-high-performance lightweight cementitious composite

[h] Fly ash cenosphere lightweight aggregate

[i] Expanded clay lightweight aggregate

[j] Expanded shale lightweight aggregate

[k] Sintered fly ash lightweight aggregate

[l] Hollow glass microsphere

[m] Oil palm shell

[n] Polyethylene (PE)

[o] Polyvinyl Alcohol (PVA)

[p] Polypropylene (PP)

[q] Cloud concrete stone

their addition does not produce sufficient enhancement in the compressive (8%) strength of L-FRCCs, it significantly enhances both the flexural (29%) and tensile (38%) strengths of L-FRCCs. Among the various fibers, the addition of steel fibers generally enhances the mechanical properties of L-FRCCs significantly but decreases the workability by approximately 22% (Li et al., 2021a; Mo et al., 2014; Shafigh et al., 2022; Tang, 2020). Balendran et al. (Balendran et al., 2002) also reported that L-FRCCs can exhibit greater energy absorption capacity and impact strength compared to normal LWC, and utilizing a high volume of steel fiber can significantly improve the strength and ductility of LWC.

This review paper explores strategies for achieving high SE and superior material and mechanical performance of L-FRCCs by analyzing previous experimental results on L-FRCCs. This review distinguishes itself from earlier papers that summarized the overall test results of L-FRCCs by providing a detailed method for producing UL-FRCCs with superior performance. It systematically organizes and analyzes previous experimental results that meet a specified strength threshold. The specific objectives are (1) to analyze the effects of different LWAs, fibers, and matrices on the material and mechanical properties of L-FRCCs, and (2) to propose a suitable strategy for enhancing both the structural efficiency and mechanical properties of L-FRCCs, thereby facilitating the development of novel UL-FRCCs.

2 Materials

The mechanical performance of L-FRCCs is significantly influenced by the types of lightweight materials and fibers it comprises. Therefore, this section provides a detailed review on the various lightweight materials and fiber types.

2.1 Lightweight materials

The manufacturing principle of L-FRCCs involves the incorporation of air into cementitious composites. Based on the air incorporation method, lightweight materials may be categorized into LWAs and foaming agents (Abid et al., 2024; Liao et al., 2025). LWAs consist of solid raw materials with inherent voids within them, which enable air to be incorporated into the matrix. Foaming agents enable the direct incorporation of air or gas bubbles into the interior of cement composite materials (Abid et al., 2024; Chiadighikaobi, 2019; Dawood & Hamad, 2013; Gencel et al., 2022; R. SWAMY,, et al., 1982; Rico et al., 2017; Xiang et al., 2022; Zhao et al., 2019).

Figure 1 illustrates various lightweight materials, including LWAs and foaming agents, and Table 1 lists the main parameters of lightweight materials used in L-FRCCs. Notably, LWAs are typically classified into

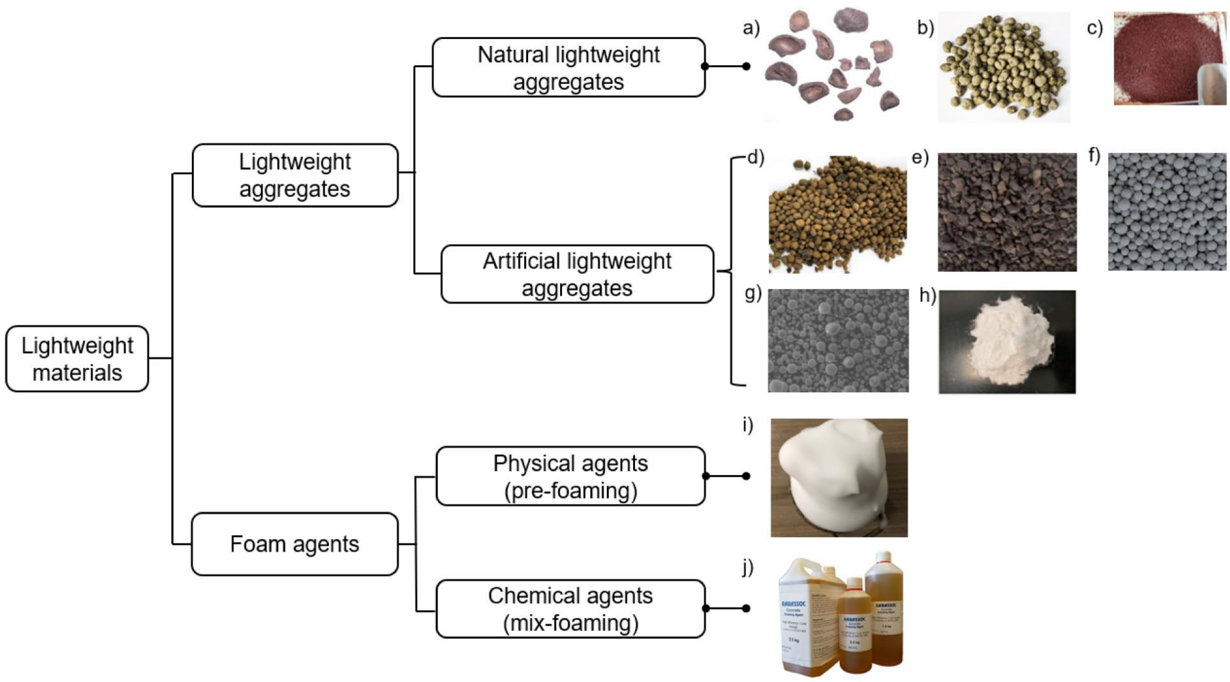

a) Oil palm shell (Yew et al., 2015)
b) Pumice (Mailyan et al., 2021)
c) Scoria (Alanazi et al., 2022)
d) Expanded clay (Chiadighikaobi, 2019)
e) Expanded shale (Zhao et al., 2019)
f) Sintered fly ash (Xiang et al., 2022)
g) Cenosphere (Yu et al., 2021)
h) HGM (Guo et al., 2023)
i) Physical foam agent (Swamy, 1982)
j) Chemical foam agent (Raj et al., 2019)

Fig. 1 Lightweight aggregates and foam agents

natural and artificial LWAs based on the type of raw materials used and production methods. Natural aggregates include pumice (Mailyan et al., 2021; Shcherban' et al., 2021), oil palm shell (Arel & Shaikh, 2018; Hosen et al., 2022; Mo et al., 2014; Shafigh et al., 2011; Yahaghi et al., 2016; Yap et al., 2016; Yew et al., 2015), and scoria (Alanazi et al., 2022; Hossain, 2004; Yu et al., 2021), whereas artificial LWAs include expanded clay (Altalabani et al., 2020; Caratelli et al., 2016; Chiadighikaobi, 2019; Esmaeili et al., 2023; Frazão et al., 2018; Gao et al., 1997; Iqbal et al., 2015; Lu et al., 2021b; Shafigh et al., 2022; Zhang et al., 2024), expanded shale (Alanazi et al., 2022; Caratelli et al., 2016; Chen & Liu, 2005; Choi et al., 2014; Frazão et al., 2018; Güneyisi et al., 2013; Liu et al., 2019a; Lu et al., 2021a; Mailyan et al., 2021; Meng et al., 2023; Poongodi & Murthi, 2020; Xie et al., 2022; Zeng et al., 2020; Zheng et al., 2019, 2025; Shen et al.2020b).), sintered fly ash (Balendran et al., 2002; Jiang et al., 2024; Kayali et al., 2003; Li et al., 2016; Xiang et al., 2022; Zeng et al., 2020), cenosphere (Gondokusumo et al., 2021; Lu et al., 2022b; Sohel et al., 2018; Wang et al., 2013; Yu et al., 2021), and HGM (Dahal et al., 2022; Guo et al., 2023; Lu et al., 2021a, 2022a, 2022b). Usually, foaming agents are classified into chemical and physical agents based on their processing methods (Ramamurthy et al., 2009; Swamy et al., 1982).

Natural LWAs are derived from natural sources; for example, scoria (Aslani et al., 2019; Alanazi et al., 2022; Hossain, 2004; Yu et al., 2021) and pumice (Mailyan et al., 2021; Shcherban' et al., 2021) are formed by the rapid cooling of lava during volcanic eruptions, and oil palm shells (OPS) (Arel & Shaikh, 2018; Hosen et al., 2022; Mo et al., 2014; Shafigh et al., 2011; Yahaghi et al., 2016; Yap et al., 2016; Yew et al., 2015) are typically agricultural by-products. Artificial LWAs, wherein voids are intentionally generated through heating and cooling processes, include expanded shale (Alanazi et al., 2022; Caratelli et al., 2016; Chen & Liu, 2005; Choi et al., 2014; Frazão et al., 2018; Güneyisi et al., 2013; Liu et al., 2019a; Lu et al., 2021a; Mailyan et al., 2021; Meng et al., 2023;

Poongodi & Murthi, 2020; Xie et al., 2022; Zeng et al., 2020; Zheng et al., 2019, 2025), expanded clay (Altalabani et al., 2020; Caratelli et al., 2016; Chiadighikaobi, 2019; Esmaeili et al., 2023; Frazão et al., 2018; Gao et al., 1997; Iqbal et al., 2015; Lu et al., 2021b; Shafigh et al., 2022; Zhang et al., 2024), sintered fly ash (Balendran et al., 2002; Jiang et al., 2024; Kayali et al., 2003; Li et al., 2016; Xiang et al., 2022; Zeng et al., 2020), cenospheres (Gondokusumo et al., 2021; Lu et al., 2022b; Sohel et al., 2018; Wang et al., 2013; Yu et al., 2021), and HGM (Dahal et al., 2022; Guo et al., 2023; Lu et al., 2021a, 2022a, 2022b). In particular, HGMs and high-strength LWAs have been recently developed and utilized as lightweight materials for producing UL-FRCCs (Dahal et al., 2022; Guo et al., 2023; Lu et al., 2021a, 2022a, 2022b).

Foam concrete is a cement mortar wherein air bubbles are introduced using suitable foaming agents (Raj et al., 2019). Foaming agents are classified into physical and chemical agents based on their mixing method, such as the addition of pregenerated bubbles during mixing. Chemical agents generate bubbles through chemical reactions during cement hydration by releasing reactive solid particles or gases (Raj et al., 2019; Rashad, 2018). Typically, lightweight foam cementitious composites utilizing foaming agents contain more voids than LWA cementitious composites, resulting in a lower density (Rashad, 2018). Consequently, lightweight foam cementitious composites may exhibit superior insulation and fire resistance compared to LWA cementitious composites (Dawood & Hamad, 2013; Gencel et al., 2022). However, the mechanical resistance of lightweight foam cementitious composites is lower than that of LWA cementitious composites (Dawood & Hamad, 2013; Gencel et al., 2022). (Table 2)

2.2 Fiber type

Figure 2 illustrates various fibers (Choi et al., 2014; Poongodi & Murthi, 2020; Wei et al., 2020; Ye et al., 2020; Zeng et al., 2020), which are categorized as either artificial or natural fibers, and Table 3 specifies the properties of fibers used in L-FRCCs. Artificial fibers include steel (Abid et al., 2024; ACI Committee, 2010, 2014; Balendran et al., 2002; Caratelli et al., 2016; Choi et al., 2014; Dawood & Hamad, 2013; Esmaeili et al., 2023; Frazão et al., 2018; Gondokusumo et al., 2021; Güneyisi et al., 2013; Hossain, 2004; Hussein et al., 2020; Iqbal et al., 2015; Kayali et al., 2003; Li et al., 2022, 2025; Liao et al., 2025; Liu et al., 2019a; Lu et al., 2021a, 2022b; Mailyan et al., 2021; Mo et al., 2014; Poongodi & Murthi, 2020; Rashad, 2018; Rico et al., 2017; Şahmaran et al., 2009; Shafigh et al., 2022; Shcherban' et al., 2021; Shen et al., 2020a, 2021; Shi et al., 2024; Sohel et al., 2018; Wang & Wang, 2013; Wang et al., 2013; Xiang et al., 2022; Xu et al., 2010; Yap et al., 2016; Ye et al., 2020; Zeng et al., 2020; Zhang et al., 2024, 2025; Zheng et al., 2025), glass (Dawood & Hamad, 2013; Shcherban' et al., 2021), carbon (Liu et al., 2019a, 2019b; Wei et al., 2020; Wu et al., 2019), and polymeric (Arel & Shaikh, 2018; Balendran et al., 2002; Gao et al., 1997; Gondokusumo et al., 2021; Güneyisi et al., 2013; Guo et al., 2023; Kayali et al., 2003; Li et al., 2016, 2022; Liao et al., 2025; Liu et al., 2019b; Meng et al., 2023; Rashad, 2018; Shen et al., 2020a; Wang et al., 2013; Wei et al., 2020; Wu et al., 2021; Xu et al., 2010; Yahaghi et al., 2016; Yew et al., 2015; Zheng et al., 2019) fibers, whereas natural fibers include basalt (Abid et al., 2024; Chiadighikaobi, 2019; Gencel et al., 2022; Mailyan et al., 2021; Zeng et al., 2020) and banana (Poongodi & Murthi, 2020) fibers. Fiber reinforcement generally leads to a bridging effect within the matrix, which reduces the crack width and increases the energy-absorption capacity of cement composites when subjected to loads. The addition of short fibers significantly increases the impact, flexural, and tensile strengths of lightweight cementitious composites (Jiang et al., 2024; Li et al., 2016; Liao et al., 2025; Tang, 2020; Yew et al., 2015; Zhang et al., 2025; Zheng et al., 2025). In addition, numerous studies have analyzed the effects of fiber shape, fiber length, and fiber diameter (Fig. 2 and Table 3) on the material and mechanical properties of L-FRCCs (Altalabani et al., 2020; Caratelli et al., 2016; Li et al., 2021a; Ye et al., 2020; Yew et al., 2015).

The enhancement of the mechanical resistance of cementitious composites induced by the bridging effect of these fibers becomes more pronounced in lightweight cementitious composites because lightweight cementitious composites typically exhibit lower mechanical resistance than conventional cementitious composites (Balendran et al., 2002). The addition of 1.2 vol.% steel fibers to conventional cementitious composites results in an increase in the flexural strength by 69%, tensile strength by 56%, and shear strength by 65%, whereas the addition of 1.2 vol.% steel fibers to lightweight cementitious composites increases the flexural strength by 107%, tensile strength by 98%, and shear strength by 43% (Choi et al., 2014). Furthermore, the addition of 1.5 vol.% vinylon fibers to conventional cementitious composites results in an increase in the flexural strength by 72%, tensile strength by 53%, and shear strength by 39%, whereas the addition of 1.5 vol.% vinylon fibers to lightweight cementitious composites increases the flexural strength by 250%, tensile strength by 104%, and shear strength by 46% (Choi et al., 2014).

Steel fibers are the most used reinforcement in L-FRCCs and utilized in various shapes, such as hooked, smooth, and twisted shapes. Owing to their inherently high strength compared to other fibers, they are extensively utilized in L-FRCCs. Due to the high density of

Table 2 Properties of lightweight materials used in L-FRCCs

Types of lightweight materials	Shape	Bulk density (kg/m³)	Cylinder compressive strength (MPa)	Crushing strength (MPa)	Particle size (mm)	Water-absorption capacity in 1 h (%)	Porosity (%)	Ref
ECLA[i]	Round but irregular	810	–	–	≤ 15	10	–	Gao et al. (1997)
ECLA	Round but irregular	810	–	–	4–8	8.2	–	Iqbal et al. (2015)
ECLA	Round but irregular	650	–	8.0	2–10	15	–	Altalabani et al. (2020)
ECLA	Round but irregular	713	–	–	12.5	14.95	72.6	Esmaeili et al. (2023)
ECLA	Round but irregular	780	–	–	12.5	17.68	–	Shafigh et al. (2022)
ECLA	Round	–	–	–	1–3	–	–	Zhang et al. (2024)
SFLA[k]	Spherical	725	6.6	–	5–20	5.8	–	Li et al. (2016)
SFLA	Spherical	877	12.1	–	5–10	8.1	–	Zeng et al. (2020)
SFLA	Spherical	1020, 1055	19.6, 27.5	–	6–10, 11–15	14.4, 15.8	–	Xiang et al. (2022)
SFLA	Spherical	1850	15	–	2.36–4.75	–	–	Meng et al. (2023)
SFLA	Spherical	970	–	–	5–20	12.25	–	Jiang et al. (2024)
ESLA[j]	Round	770	–	6.6	–	–	43	Wang and Wang (2013)
ESLA	–	888, 816	8.3, 7.3	–	20	7.65, 8.5	–	Zhao et al. (2016)
ESLA	–	–	–	–	0.6–1.25	-	51.6	Liu et al. (2019a)
ESLA	Quasi-spherical, irregular	1019, 869, 755, 856, 860	13.2, 10.4, 5.9, 6.2, 6.9	–	5–16	9.1, 7.5, 10.1, 2.6	–	Wu et al. (2019)
ESLA	Spherical	845	6.1	–	2.36–16	2.0	42.1	Zheng et al. (2019)
ESLA	Angular	869	–	6.9	–	2.2	43.12	Wei et al. (2020)
ESLA	–	750	6.2	–	5–16	3.2	–	Ye et al. (2020)
ESLA	–	–	–	–	0.15–1.18	–	–	Shen et al. (2020a)
ESLA	Shell	525, 539	–	0.76, 4.58	–	13.4, 14.2	63.9, 68	Lu et al. (2021b)
ESLA	Spherical	994	11.8	–	5–16	3.8	–	Li et al. (2021a)
ESLA	Angular and irregular	–	–	–	0.00–4.75	15.8	–	Gondokusumo et al. (2021)
ESLA	-	1270	–	–	15	10.3	–	Choi et al. (2014)
ESLA	Spherical	1400	6.4	–	–	10	–	Abid et al. (2024)
ESLA	Spherical	1366	–	8.66	5–10	7.50	–	Liao et al. (2025)
ESLA	Spherical	653	5.6	–	5–20	3	–	Li et al. (2025)
FCLA[h]	Cenospheres	870	–	–	0.01 – 0.3	–	–	Wang et al. (2013)
FCLA	Cenospheres	900	–	–	0.11	–	–	Yu et al. (2021)
FCLA	Cenosphere	418	–	–	0.05–0.1	–	–	Zhang et al. (2025)
Ceramsite sand	Spherical	1580	–	–	2.36 – 5	–	–	Xie et al. (2022)
HGM[l]	Spherical	420	–	–	0.01– 0.1	–	–	Lu et al. (2021a)
HGM	Spherical balls	420, 710, 750	–	–	0.031, 0.035, 0.21	–	–	Lu et al. (2022b)
HGM	Spherical	-	–	–	0.017	–	–	Dahal et al. (2022)
HGM	Spherical	460	–	–	0.02	–	–	Guo et al. (2023)

Table 2 (continued)

Types of lightweight materials	Shape	Bulk density (kg/m^3)	Cylinder compressive strength (MPa)	Crushing strength (MPa)	Particle size (mm)	Water-absorption capacity in 1 h (%)	Porosity (%)	Ref
HGM	Spherical	750	–	–	0.2–0.4	–	–	Zhang et al. (2025)
OPS[m]	Concave and convex	635	–	–	14	24.3	–	Mo et al. (2014)
OPS	Concave and convex	635	–	–	15	24.3	–	Yap et al., 2016)
OPS	–	673	–	–	10	21	–	Yahaghi et al. (2016)
OPS	–	607	–	–	12.5	23.16	–	Arel and Shaikh (2018)
OPS	–	-	–	–	5– 12.5	–	–	Hosen et al. (2022)
Pumice	Round but irregular	1400	–	–	5–10	–	–	Mailyan et al. (2021)
Pumice	Round but irregular	612	–	0.8	5–20	–	53	Shcherban' et al. (2021)
Stalite	Angular	849	–	5.26	13	6.03	–	Liu et al. (2021)
Bentonite clay	–	543	–	–	10	12.9	–	Hussein et al. (2020)
Reservoir sludge	–	707.5	–	3.6	–	4.9	–	Tang (2020)
Scoria	–	1150	–	–	2–64	35.60	–	Hossain (2004)
Cloud concrete stone	–	1638	–	–	5–16	–	–	Zheng et al. (2025)
High strength core shell	Spherical	870	–	10.87	5–10	15.58	–	Liao et al. (2025)

[h] Fly ash cenosphere lightweight aggregate

[i] Expanded clay lightweight aggregate

[j] Expanded shale lightweight aggregate

[k] Sintered fly ash lightweight aggregate

[l] Hollow glass microsphere

[m] Oil palm shell

steel, when the amount of steel fibers is increased, the density of L-FRCCs containing steel fibers increases significantly but the workability decreases (Mo et al., 2014).

Polymeric fibers, which possess a lower density than steel fibers, have also been widely used. Representative polymeric fibers include polypropylene (PP), polyethylene (PE), and polyvinyl alcohol (PVA) fibers. In contrast to steel fibers, polymeric fibers possess relatively lower elastic moduli and densities but exhibit notable characteristics such as superior resistance to acids/alkalis (Yew et al., 2015).

Natural fibers such as basalt and banana fibers are obtained from natural sources and processed for reinforcement in L-FRCCs. These fibers exhibit relatively lower reinforcing effects and mechanical properties than other fibers. However, they offer advantages such as cost-effectiveness and ease of application (Chiadighikaobi, 2019; Li et al., 2025; Mailyan et al., 2021; Shi et al., 2024; Trabelsi & Kammoun, 2020).

3 Fresh and hardened properties of L-FRCCs

3.1 Workability

The workability of L-FRCCs varies significantly depending on the type and proportion of LWAs used. Reported slump values of L-FRCCs range from as low as 5 mm to as high as 255 mm, whereas slump flow values span from 80–790 mm, reflecting the broad impact of mixture composition on fresh-state behavior (Alanazi et al., 2022; Meng et al., 2023). Incorporating LWAs often improves workability compared to composites without them, primarily because of the reduced packing density and different surface characteristics of LWAs (Alanazi et al., 2022). For instance, utilizing scoria as a fine LWA increases the slump flow from 184.3 mm to 210.3 mm. The replacement ratio of fine aggregate with scoria rose from 0

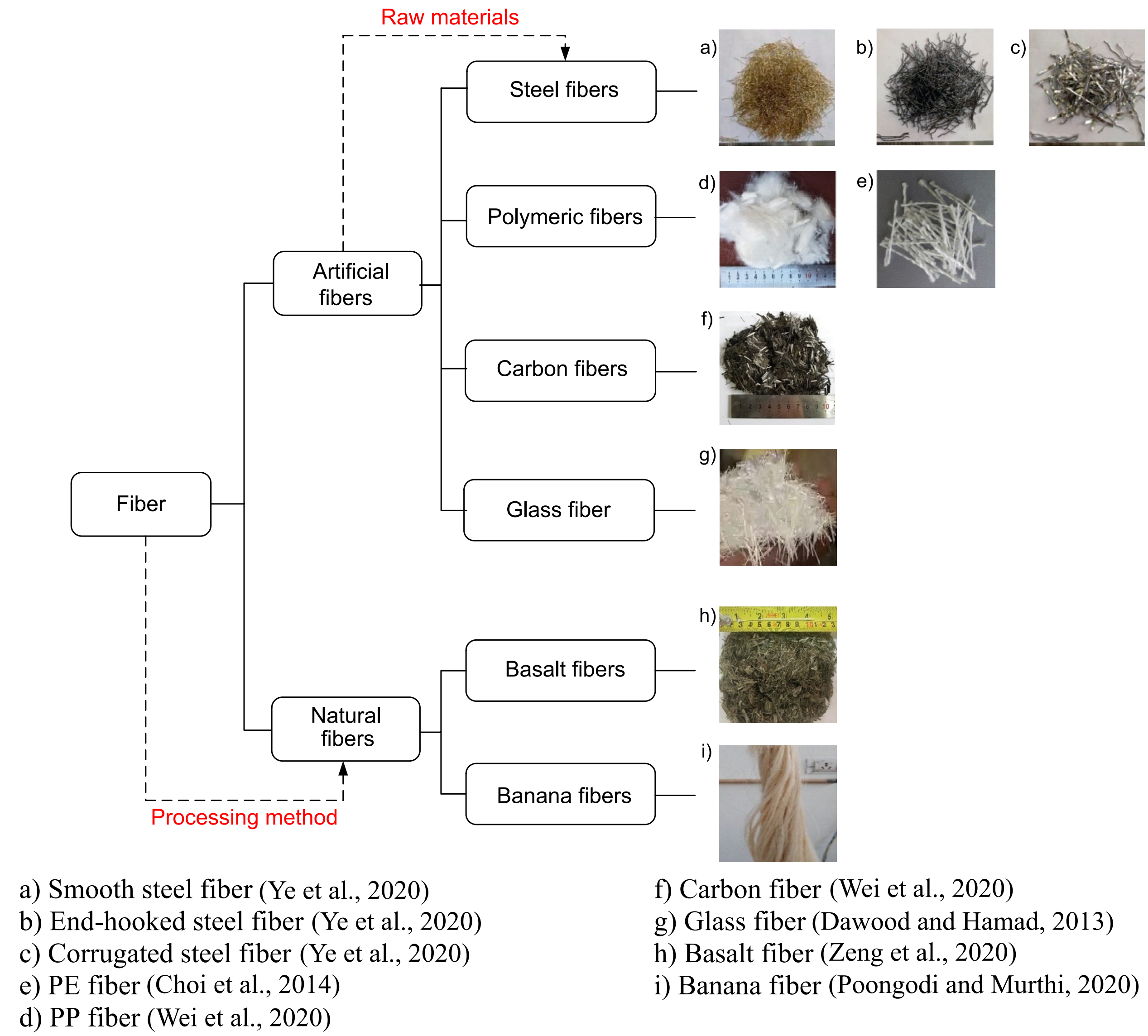

Fig. 2 Various types of fiber

to 15% by weight (Alanazi et al., 2022). Conversely, the use of fly ash ceramic aggregates led to a reduction in slump flow from 260 to 80 mm as the replacement level increased from 25 to 75% in the volume of fine aggregates (Meng et al., 2023). Meng et al. (Meng et al., 2023) highlighted that the workability of lightweight concrete is more strongly influenced by the aggregate's type, shape, and water absorption properties than by its dosage. For example, small quasi-spherical LWAs with low water-absorption characteristics may positively affect the workability of L-FRCCs.

Generally, the workability of L-FRCCs is lower than that of a normal LWC. Figure 3 shows the slump of L-FRCCs according to the volume content of the fibers (Mo et al., 2014; Shafigh et al., 2011, 2022; Wei et al., 2020; Yahaghi et al., 2016; Yap et al., 2016; Yew et al., 2015; Zhao et al., 2016). The results for carbon, PP, milling steel, and hooked-end steel fibers are also demonstrated. As illustrated in the figure, the slump generally decreased as the volume content of the fibers increased; this can be attributed to the fibers holding more cement paste around their surface owing to the large surface area, resulting in an increase in the viscosity of the cement paste and consequently reducing the workability of L-FRCCs (Alanazi et al., 2022; Chen & Liu, 2005; Li et al., 2021a). Moreover, the grid spacing between the materials in the matrix increases with the fiber content, resulting in decreased fluidity of the cementitious

Table 3 Properties of fiber used in L-FRCCs

Fiber type	Fiber shape	Length (mm)	Diameter (mm)	Fiber volume content (vol.%)	Tensile strength (MPa)	Elastic modulus (GPa)	Density (kg/m^3)	Ref
Steel	Rectangular	20, 25, 30	0.435, 0.431, 0.439	0, 0.6, 1.0, 1.5, 2.0	–	–	–	Gao et al. (1997)
Steel	Straight	15	0.25	5–20	–	–	–	Balendran et al. (2002)
Steel	Enlarged ends	32	0.64	0, 0.5, 1.0, 1.5, 2.0	600	–	–	Wang & Wang (2013)
Steel	Milling	36	1.35	0.4, 0.8, 1.2, 1.6, 2.0	–	–	–	Zhao et al. (2016)
Steel	Smooth	13	0.2	0.3, 0.6, 0.9	2500–3000	200	7800	Wu et al. (2019)
Steel	Wavy	30	0.75	0, 0.5, 1.0, 2.0	> 600	–	–	Zheng et al. (2019)
Steel	Smooth, hooked, and corrugated	13, 25, 30	0.2, 0.5, 0.8	0.5, 1.0, 1.5, 2.0	–	–	–	Ye et al. (2020)
Steel	Straight	13	0.22	2.0	–	–	–	Shen et al. (2020a)
Steel	Straight	13	0.22	1.5	–	–	–	Lu et al. (2021b)
Steel	Hooked and smooth	13, 35	0.2, 0.5	0, 0.25, 0.5, 0.75	> 1100	–	7850	Li et al. (2021a)
Steel	Smooth	13	0.2	1.5, 2.5	–	–	7800	Xie et al. (2022)
Steel	Straight	13	0.22	1.5	–	–	7800	Lu et al. (2021a)
Steel	Straight	13	0.22	2.0	–	–	–	Lu et al. (2022b)
Steel	Smooth	13	0.22	-	> 2850	–	–	Li et al. (2022)
Steel	Straight	13	0.22	0.5–2.5	-	–	–	Meng et al. (2023)
Steel	Hooked	35	0.538	0.25–1.0	1100	205	–	Yap et al. (2016)
Steel	Hooked	35	0.54	0.25–1.5	1200	210	7840	Shafigh et al. (2022)
Steel	Hooked	35, 50	0.55, 0.75	0.75–1.25	1200	–	7850	Gondokusumo et al. (2021)
Steel	Straight	19.5	0.2	–	> 2450	–	7850	Dahal et al. (2022)
Steel	Hooked	60, 30	0.55, 0.75, 0.92	0.35, 0.7, 1.0, 1.5	1050, 1160, 1345	–	7850	Güneyisi et al. (2013)
Steel	–	8, 16	0.2	1.5	2200	–	7850	Arel & Shaikh (2018)
Steel	Straight	13	0.2	0–1.25	2500	–	–	Iqbal et al. (2015)
Steel	Enlarged ends	18	0.48	0.56, 1.13, 1.7	–	–	–	Kayali et al. (2003)
Steel	Hooked	35	0.54	0–1.5	1130	200	7840	Hosen et al. (2022)
Steel	Hooked	30	0.8	0–1.15	> 990	200	–	Esmaeili et al. (2023)
Steel	Hooked	19.5	0.2	1.0	2500	200	7800	Alanazi et al. (2022)
Steel	Hooked	30	0.62	0.4, 0.8, 1.2	1000	200	7850	Choi et al. (2014)
Steel	–	13	0.22	3.0	2850	–	–	Zhang et al. (2024)
Steel	Smooth	13	0.12	2.0	2900	116	970	Zhang et al. (2025)
Steel	Smooth	13.2	0.21	0.5–1.5	3296		7800	Liao et al. (2025)
Carbon	Straight round bundled filament	8–10	0.007	0.2, 0.4	> 4000	240	1800	Wei et al. (2020)
Carbon	Straight round bundled filament	6	0.007	0.3, 0.6, 0.9	4000- 4500	240	1760	Wu et al. (2019)

Table 3 (continued)

Fiber type	Fiber shape	Length (mm)	Diameter (mm)	Fiber volume content (vol.%)	Tensile strength (MPa)	Elastic modulus (GPa)	Density (kg/m^3)	Ref
Carbon	–	1	0.0073	0.4	4650	230	1820	Zhang et al. (2025)
PP[p]	Corrugated surface	30	0.91	0, 0.53, 0.74, 0.95, 1.16, 1.37	543	9.88	950	Li et al. (2016)
PP	–	12	–	0, 0.1, 0.2, 0.3	400	–	900	Yahaghi et al. (2016)
PP	Straight	12, 39	0.032, 0.78	0, 0.22, 0.33, 0.44, 0.66	272, 470	3.5, 3.6	910	Altalabani et al. (2020)
PP	Straight	12	0.05	0.1	300	–	900	Tang (2020)
PP	Fibrillated	19	0.016	0.1–0.3	400	3.9	900	Shafigh et al. (2022)
PP	Fibrillated	19	0.125	0.28, 0.56, 1.0	–	–	–	Kayali et al. (2003)
PP	Straight round bundled filaments	15–22	0.08	0.2, 0.4	> 400	4.2	910	Wei et al. (2020)
Basalt	–	6	0.0174	0–1.5	2000	85	–	Zeng et al. (2020)
Basalt	–	12	0.016	1.5, 2.0, 2.5	3200	120	2600	Mailyan et al. (2021)
Basalt	Twisted	–	–	0.1, 0.3, 0.5	1311	45	1780	Shi et al. (2024)
Basalt	Shortcut	12	0.0174	–	2180	87.2	2699	Abid et al. (2024)
Bamboo	Straight	10–40	-	0.25, 0.5, 0.75	–	–	–	Li et al. (2025)
PVA[o]	Straight	8	0.04	0, 0.3, 0.6, 0.9, 1.2	1600	40	1300	Xu et al. (2010)
PVA	–	6	0.027	0.9	1600	39	1300	Sohel et al. (2018)
PE[n]	–	18	0.024	2	2400	–	970	Yu et al. (2021)
PE	–	6	0.018	–	3400	151	970	Guo et al. (2023)
PE	Yarned	30	0.68	0.5, 1.0, 1.5	1870	43	970	Choi et al. (2014)
PE	–	13	0.12	1.0	2850	210	108.3	Zhang et al. (2025)
Vinylon	Straight	30	0.66	0.5, 1.0, 1.5	900	23	1300	Choi et al. (2014)
Polyolefin polymer	Straight and embossed	30	–	0.5, 1.0, 1.5, 2.0	550	–	920	Liu et al. (2021)
Glass	–	12	0.013	3.0 wt.% by cement	3100	72	2600	Shcherban' et al. (2021)

[n] Polyethylene (PE)

[o] Polyvinyl Alcohol (PVA)

[p] Polypropylene (PP)

composites (Meng et al., 2023). With 1.5 vol.% of hooked-end steel fiber (aspect ratio = 65), the slump reduction was the highest (from 70 to 5 mm) (Shafigh et al., 2022) owing to the larger surface area compared to other fibers. However, 0.1 vol.% of PP fiber didn't produce any reduction (Shafigh et al., 2022).

Figure 4 depicts the slump and slump flow of the L-FRCCs according to the different fiber types with the same volume content (1 vol.%) (Chen & Liu, 2005). The steel fibers result in a significant decrease in the slump and slump flow from 240 to 80 mm and 540 to 220 mm, respectively, whereas the PP fibers produce the lowest reduction in both the slump and slump flow from 240 to 190 mm and 540 to 480 mm, respectively; this may be primarily attributed to the relatively higher stiffness and density of steel fibers than others (Chen & Liu, 2005). Li et al. (2021a) reported that steel fibers with a higher stiffness compared to other fibers resulted in a higher resistance between the aggregates and fibers, a primary factor contributing to the high slump reduction. Conversely, Swamy et al. (1982) reported that a smaller aspect ratio of the fibers significantly improved the workability of L-FRCCs. They demonstrated that straight steel fibers with a smaller aspect ratio of 50 produced the highest slump (85 mm) owing to the smaller surface area and superior compatibility, whereas hooked-end steel fibers

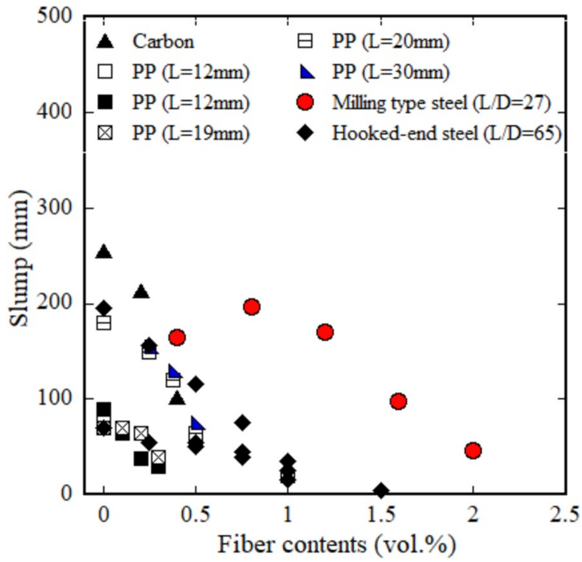

Fig. 3 Effects of fiber contents on the slump of L-FRCCs

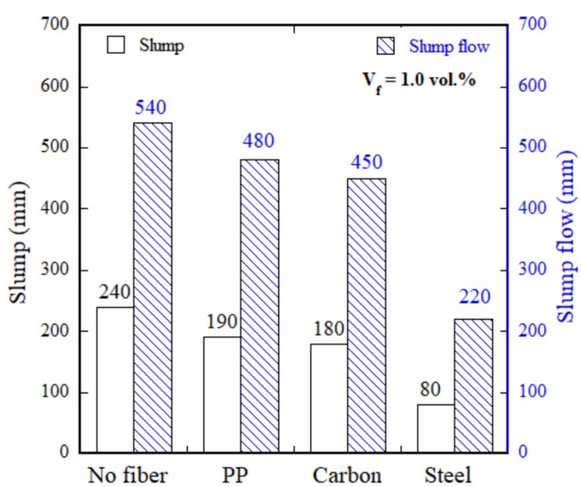

Fig. 4 Effects of fiber types on slump and slump flow values of L-FRCCs

with a higher aspect ratio of 100 produced the lowest slump (8 mm) owing to the large surface area.

3.2 Density

The density of L-FRCCs ranges from 1440 to 2150 kg/m^3, as demonstrated in Table 1. As LWAs are the most extensively used material for reducing the density of L-FRCCs, the void ratio and specific gravity of LWAs significantly impact the density of L-FRCCs. In addition to artificial LWAs, such as expanded clay (specific gravity 0.96–2.63) and expanded shale (specific gravity 1.07–2.52), which are mainly used to replace coarse or fine aggregates (Guo et al., 2023; Liao et al., 2025; Lu et al., 2021b; Rashad, 2018; Shi et al., 2024), lighter L-FRCCs have been produced by substituting cement and binders with cenospheres (specific gravity 0.75) or HGM (specific gravity 0.42–0.46) (Dahal et al., 2022; Gondokusumo et al., 2021; Guo et al., 2023; Lu et al., 2021a, 2022a, 2022b; Wang et al., 2013; Yu et al., 2021; Zhang et al., 2025). In particular, HGM (with an average particle size of 35–36 μm, crushing strength greater than 80 MPa, and specific gravity of 0.42–0.46) is primarily utilized to substitute 10–50 vol.% of cement and binders based on its high pozzolanic reactivity (Dahal et al., 2022; Guo et al., 2023; Lu et al., 2021a, 2022a; Zhang et al., 2025). This material enables the production of UL-FRCCs with very low density (1825–2120 kg/m^3) and high strength (100–170 MPa).

Figure 5 illustrates the effect of various types of LWA on the density of L-FRCCs (Guo et al., 2023; Lu et al., 2021a, 2021b). Replacing with 50% LWA content led to a lower density (1825–2249 kg/m^3) compared to that of normal cementitious composites (2300–2500 kg/m^3). In particular, using HGM with a specific gravity of 0.42 produced the lowest density of 1825 kg/m^3 owing to its ultra-lightweight characteristics and hollow internal structure. However, utilizing expanded clay with a specific gravity of 2.63 produced the highest density of 2249 kg/m^3. Lu et al. (2021a) reported that HGM could replace binder materials owing to the high pozzolanic reactivity and similar composition to binders, which may further decrease the density of L-FRCCs.

Figure 6 illustrates the density of L-FRCCs with expanded clay and expanded shale according to different fine aggregate replacement percentages between 50 and 200% (Lu et al., 2021b). Both expanded clay and shale noticeably decreased the density by up to 9.3–34.3%, as illustrated in Fig. 6. The similar specific gravities of the two LWAs generated similar densities of L-FRCCs. In particular, the replacement of all fine aggregates (replacement percentage of 100%) with expanded clay and shale resulted in a notable decrease in the density by 26.2% and 24.6%, respectively, because the density of conventional fine aggregates (2530 kg/m^3) was considerably greater than that of others. However, after all the fine aggregates were replaced (replacement percentage of 150% and 200%), the reductions in density were not remarkable. A similar tendency was observed in several studies (Guo et al., 2023; Lu et al., 2021a; Şahmaran et al., 2009; Xie et al., 2022; Yu et al., 2021).

The use of steel fibers in L-FRCCs produced a higher density of L-FRCCs than other carbon and/or polymeric fiber reinforced L-FRCCs (Choi et al., 2014; Guo et al., 2023; Kayali et al., 2003; Liao et al., 2025; Liu et al., 2019a, 2019b; Tang, 2020; Wang et al., 2013). Mo et al. (2014) compared the densities of L-FRCCs reinforced with steel and polymeric fibers. They revealed that when the same

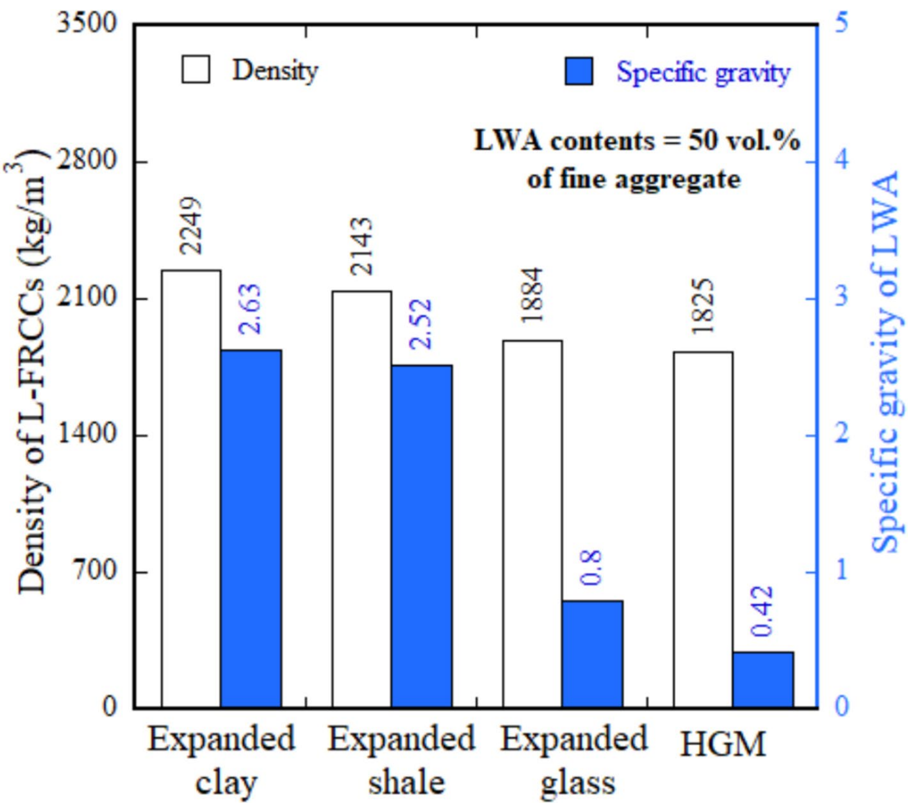

Fig. 5 Effects of LWA types on the density of L-FRCCs

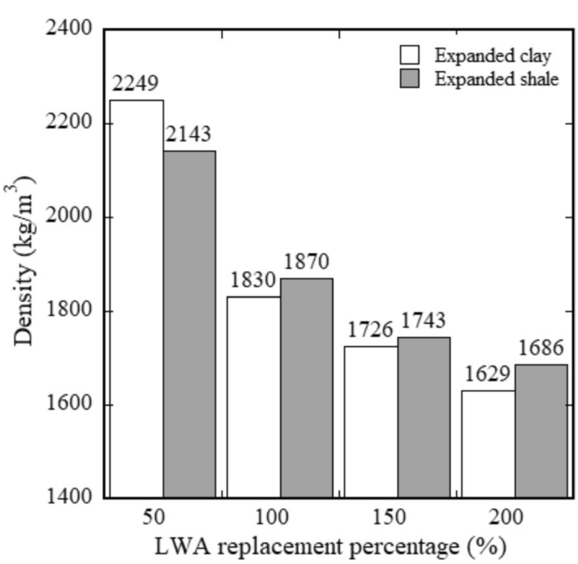

Fig. 6 Effects of LWA contents on the density of L-FRCCs

amount of oil palm shell LWA was used in L-FRCCs, the steel fibers resulted in L-FRCCs with considerably higher density (1940 kg/m^3) than those reinforced with PP fibers (1700 kg/m^3). A similar tendency was observed in several studies (Guo et al., 2023; Kayali et al., 2003). Conversely, when the same amounts (0.2–0.4 vol.%) of PP and carbon fibers were used, the L-FRCCs reinforced with PP fiber exhibited lower density (1728–1730 kg/m^3) than those reinforced with carbon fiber (1825–1844 kg/m^3) (Wei et al., 2020). Wei et al. (2020) reported that the specific gravity (density) of short-length micro polymeric fibers may be lower than that of cement paste. Several studies have shown that PP fiber reinforcement results in L-FRCCs with an even lower density than those without fibers (Shafigh et al., 2022; Wei et al., 2020; Yahaghi et al., 2016; Yew et al., 2015). Furthermore, Hassanpour et al. (Hassanpour et al., 2012) reported that blending low volumes of steel and non-metallic fibers, rather than using a high volume of steel fibers alone, is more effective for producing higher SE of L-FRCCs.

Figure 7 shows the density of L-FRCCs according to different volume content of the fibers, including PP, enlarged-end steel, hooked-end steel, and straight steel fibers (Kayali et al., 2003; Liu et al., 2019b; Shafigh et al., 2022; Wei et al., 2020; Yahaghi et al., 2016; Yap et al., 2016; Yew et al., 2015). When the volume content of PP and steel fibers increased, the density of L-FRCCs with steel fibers increased, whereas that with PP fibers was not affected or even decreased.

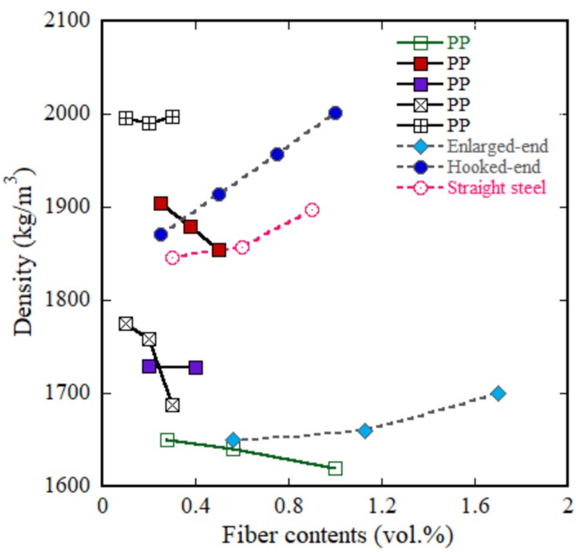

Fig. 7 Effect of fiber contents on the density of L-FRCCs

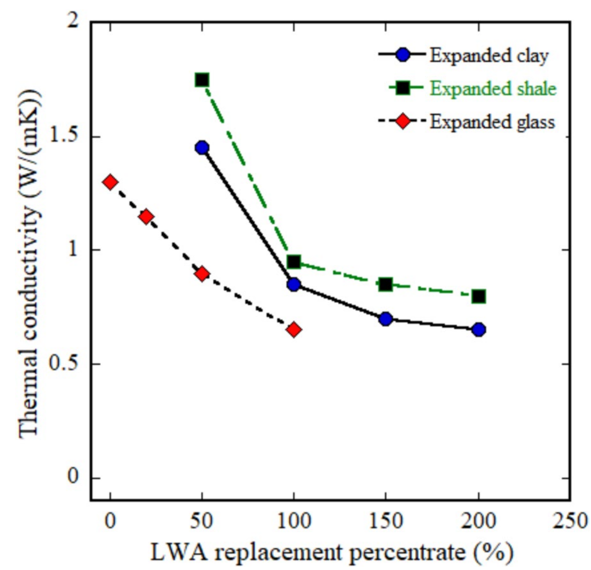

Fig. 8 Effects of LWA contents on thermal conductivity for various types of LWA

3.3 Thermal conductivity

As presented in Table 1, the thermal conductivity of L-FRCCs ranges from 0.33 to 1.22 W/mK and is generally lower than that of normal concrete (1.6–3.2 W/mK) (Rezaei et al., 2020; Yun et al., 2014). The lower thermal conductivity of L-FRCCs compared to that of normal cementitious composites originates from the specific pore systems of LWAs. For instance, an expanded clay LWA contains air-filled voids with sizes ranging from 5 to 300 μm, forming cavities. These numerous small cavities filled with air impede heat transfer within the matrix, thereby slowing the internal heat transfer (Lu et al., 2021b).

Figure 8 illustrates the thermal conductivity of L-FRCCs with different LWAs, namely expanded shale, expanded clay, expanded glass, and combined sintered fly ash and palm oil-fueled ash, as the fine aggregate replacement ratio increases (Guo et al., 2023; Lu et al., 2021b). The LWAs significantly decreased the thermal conductivity of L-FRCCs as their content increased. With the same replacement ratio, the expanded glass produced the lowest thermal conductivity (0.65 W/mK) compared to those produced by expanded clay and expanded shale (0.85 and 0.95 W/mK, respectively). Furthermore, the use of different types of lightweight material, namely palm oil-fueled ash, resulted in a further decrease in the thermal conductivity of L-FRCCs (up to 0.40 W/mK) due to the synergetic effect (Johnson Alengaram et al., 2013). The pozzolanic reactivity of palm oil-fueled ash produced additional cementitious compounds such as calcium silicate hydrate and calcium hydrate during cement hydration, which reduced the heat transfer (Johnson Alengaram et al., 2013; Nazari & Riahi, 2011). Concurrently, the porous structure of sintered fly ash introduced a high volume of entrapped air and further disrupted the pore network, thus increasing the tortuosity of heat transfer pathways (Zhang et al., 2020).

Figure 9 shows the thermal conductivity of L-FRCCs according to the volume content of PP and steel fibers (Shafigh et al., 2022). As the volume content of steel fibers increased from 0.25% to 1.5%, the thermal conductivity increased from 1.22 to 1.41 W/mK. However,

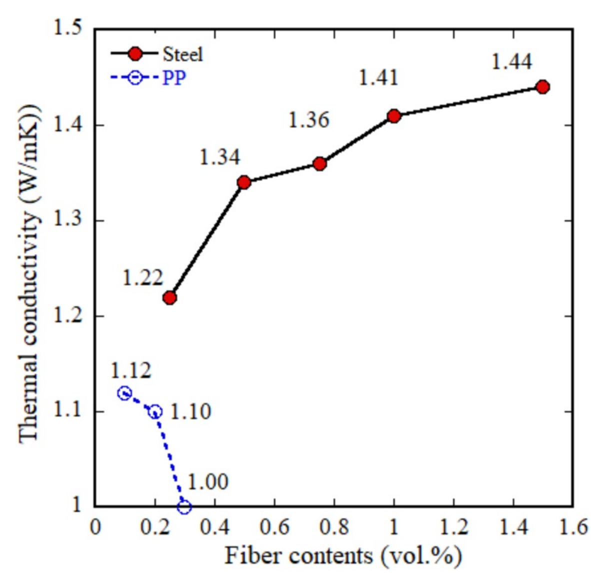

Fig. 9 Effects of fiber content on thermal conductivity of L-FRCCs

in the case of PP fibers, an increase in the volume content from 0.1% to 0.3% decreased the thermal conductivity from 1.12 to 1.0 W/mK. When using the same amounts of lightweight materials, steel fiber-reinforced L-FRCCs exhibited an average thermal conductivity that was greater than that of PP fiber-reinforced L-FRCCs by a factor of 1.3 (Shafigh et al., 2022). This variation may be attributed to the inherent thermal conductivity of the fibers (Gencel et al., 2022; Guo et al., 2023; Shafigh et al., 2022; Trabelsi & Kammoun, 2020). For instance, steel fibers generally have a higher thermal conductivity of 45 W/mK than that of PP fiber (0.26 W/mK).

3.4 Sound absorption capacity

To determine the performance of an acoustic material, the sound absorption coefficient (α) is measured. The values of α range from 0 to 1 depending on the frequency. When the material entirely reflects the incident sound energy,α is 0. Conversely, when the material completely absorbs the sound energy, α is 1. In this section, the sound absorption capacity of the LWC was reviewed based on the literature (Arenas et al., 2013; Carbajo et al., 2015a, 2015b; Hong et al., 2025; Kim & Lee, 2010; Ling et al., 2010; Mohammed et al., 2012; Neithalath et al., 2006; Sukontasukkul, 2009; Tajra et al., 2019; Tiwari et al., 2004). The LWC ultilizing crumb rubber as the aggregate exhibited potential improvement in the acoustic properties of the concrete (Ling et al., 2010; Mohammed et al., 2012; Sukontasukkul, 2009). For example, Ling et al. (Ling et al., 2010) reported that the highest sound absorption coefficient ($\alpha = 0.11$) was obtained at a frequency of 1000 Hz when 30% crumb rubber content was added. This was because the large amount of crumb rubber in the concrete increased its porosity, thereby reducing frictional losses within the pore structure. Thus, higher crumb rubber content in concrete improves the sound absorption ability. Arenas et al. (2013) found that incorporating 80% bottom ash aggregate in the LWC improved the acoustic absorption coefficient (peak value of $\alpha = 0.92$ at frequency 4000 Hz), which is attributed to the porous character of the bottom ash aggregate. Tiwari et al. (2004) reported that incorporating up to 40% lightweight cenospheres (with particle sizes between 10 and 300 μm) into asphalt concrete significantly enhanced its acoustic performance. The modified mix achieved a higher sound absorption coefficient ($\alpha = 0.3$ at frequencies between 1000 and 1600 Hz) compared to the control sample without cenospheres (α = 0.1). Carbajo et al. (2015b) found that pervious concrete incorporating vermiculite LWAs with particle size smaller than 1 mm achieved an optimal sound absorption coefficient of $\alpha = 0.92$ at 1200 Hz. In contrast, when using vermiculite aggregates with particle size larger than 1 mm, the peak absorption decreased to approximately $\alpha = 0.8$ at the same frequency. Neithalath et al. (2006) observed a maximum sound absorption coefficient of $\alpha = 0.78$ in pervious concrete made with conventional coarse aggregates. In comparison, Kim et al. (2010) reported an even higher α value of 0.96 when expanded shale was used as the coarse aggregate in pervious concrete. The α value was evaluated within the frequency range of 250–1250 Hz, which falls within the standard range used for traffic noise assessment (Kim & Lee, 2010). Lu et al. (2021a) reported that the UHP-FRCCs containing HGMs demonstrated sound absorption capability ($\alpha = 0.18$), especially within the frequency range of 500–800 Hz. This behavior can be explained by the formation of small acoustic cavities on the truncated surface of the UHP-FRCCs due to HGMs incorporated into the mixture. Recently, Hong et al. (2025) investigated the sound insulation of ultra-high-strength lightweight concrete (UHSLC) containing carbon nanotube (CNT) and various fiber types. They concluded that the UHSLC containing PE fiber improved the sound absorption capacity by 73% ($\alpha = 0.47$) compared with the control sample without fiber in the frequency range of 200–2500 Hz. Table 4 summarizes the

Table 4 Sound absorption capacity of different type of concretes

Type of concrete	Sound absorption coefficient	Frequency, (Hz)	Ref
Normal concrete	0.05–0.10	3000–5500	Carbajo et al. (2015a)
LWC ultilizing crumb rubber	0.11	1000	Ling et al. (2010)
LWC containing bottom ash aggregate	0.92	4000	Arenas et al. (2013)
Asphalt concrete containing lightweight cenospheres	0.30	1000–1600	Tiwari et al. (2004)
Pervious concrete containing vermiculite lightweight aggregates	0.92	1200	Carbajo et al. (2015b)
Pervious concrete using expanded shale as coarse aggregate	0.96	250–1250	Kim & Lee (2010)
UHP-FRCCs containing HGMs	0.18	500–800	Lu et al. (2021a)
UHSLC containing PE fiber and CNT	0.47	200–2500	Hong et al. (2025)

CNT Carbon nonotube, *UHSLC* ultra-high-strength lightweight concrete sound absorption capacity of different type of concretes. As shown, the various types of LWCs exhibited higher sound absorption capacity than normal concrete.

4 Mechanical properties of L-FRCCs

4.1 Compressive strength

The compressive strength of L-FRCCs ranges from 45 to 145 MPa, as illustrated by the data in Table 1. The compressive strength of L-FRCCs is higher than that of the normal concrete (15–62 MPa) (Rezaei et al., 2020) and lower than that of the FRCCs (150–80 MPa) (Nguyen et al., 2023), indicating that L-FRCCs can achieve mechanical performance comparable to normal concrete while offering the added benefits of reduced weight. In general, L-FRCCs containing lightweight materials with numerous internal voids typically exhibit lower compressive strengths than conventional cementitious composites (Abid et al., 2024; Balendran et al., 2002; Jiang et al., 2024; Liao et al., 2025; Yu et al., 2021). The lower compressive strength of L-FRCCs may be directly related to their density because their compressive strength generally reduces as they become lighter. Therefore, many studies have focused on developing lightweighting cementitious composites while minimizing the strength reduction.

Figure 10 shows the compressive strengths of L-FRCCs with different LWA types according to the fine aggregate or binder material replacement ratios (Lu et al., 2021b, 2022b; Şahmaran et al., 2009; Xie et al., 2022; Yu et al., 2021). As the replacement percentage increased from 0 to 200%, the compressive strength of L-FRCCs decreased by 11–68%. The use of HGM as a binder successfully minimized the reduction of compressive strength below 12% owing to their smaller size (31.3–34.7 μm) and higher crushing strength (more than 80 MPa) than general LWAs, along with their pozzolanic reactivity (Lu et al., 2022b). However, utilizing crumb rubber as a replacement for 50% fine aggregates resulted in a significant decrease in the compressive strength from 113 to 38 MPa (Yu et al., 2021). Yu et al. (2021) reported that this may be attributed to the incompatibility between crumb rubber and the matrix because the low stiffness and strength of crumb rubber significantly damaged the interfacial properties. Similarly, as the replacement rate of ceramsite sand increases, the compressive strength produces a gradually decreasing tendency. Xie et al. (2022) concluded that this was due to the ceramsite sand lacking sufficient strength and having lots of pores.

Figure 11 illustrates the compressive strengths of L-FRCCs according to different metallic fiber content, namely corrugated steel fibers, hooked-end steel fibers, rectangular steel fibers, and straight steel fibers, based on their volume content (Abid et al., 2024; Alanazi et al., 2022; ASTMC, 2017; Caratelli et al., 2016; Choi et al., 2014; Esmaeili et al., 2023; Frazão et al., 2018; Gondokusumo et al., 2021; Hong et al., 2025; Hussein et al., 2020; Iqbal et al., 2015; Kayali et al., 2003; Li et al., 2016; Liao et al., 2025; Lu et al., 2022a, 2022b; Meng et al., 2023; Mo et al., 2014; Poongodi & Murthi, 2020; Rico et al., 2017; Şahmaran et al., 2009; Shafigh et al., 2022; Shcherban' et al., 2021; Shen et al., 2020a; Xie et al., 2022; Xu et al., 2010; Yap et al., 2016; Yu et al., 2021; Zeng et al., 2020). Various steel fibers tended to gradually increase the compressive strength of the L-FRCCs as the volume fraction

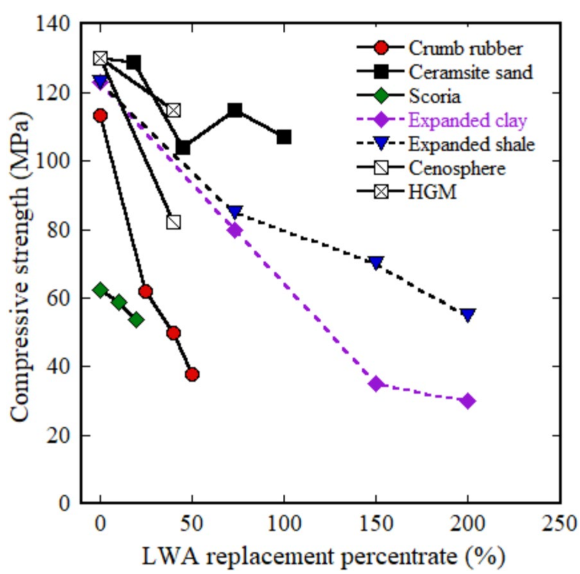

Fig. 10 Effects of LWA contents on compressive strength of L-FRCCs

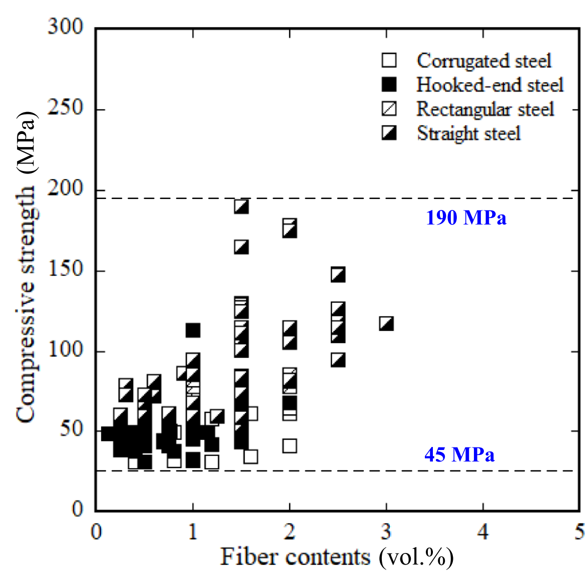

Fig. 11 Effects of metallic fiber content on compressive strength

increased (0.13–1.5 vol.%). However, the compressive strength decreased for values greater than 2.0 vol.% of steel fibers. Gao et al. (1997) reported that the uniform dispersion of fibers may be hindered beyond a certain fiber volume fraction, impeding proper densification of the cement paste, which may lead to a marginal decrease in compressive strength. They also proposed a steel fiber reinforcement ratio of less than 2.5% by volume. In addition, among the various types of steel fibers, the incorporation of straight steel fibers in the L-FRCCs resulted in a maximum compressive strength of 190 MPa owing to the large specific area (Fig. 11) compared with that of other fibers (31–113 MPa) (Lu et al., 2021a). Ye et al. (2020) reported that straight steel fibers (aspect ratio of 65) with 2.0 vol.% achieved the highest increment in compressive strength (47%); however, hooked-end steel fiber (aspect ratio = 50) and corrugated steel fiber (aspect ratio = 38) with the same volume contents resulted in an increase in the compressive strength by 22 and 12%, respectively; this trend is due to the easier dispersion of straight steel fibers within the matrix, enabling a better bonding performance between them (Ye et al., 2020). They also reported that the surface of the fibers should be roughened to maintain a strong bond with the cement paste, and the inherent strength of the fiber should not be too low.

Figure 12 shows the compressive strength of L-FRCCs with different non-metallic fibers, namely carbon, PE, and PP fibers, according to their volume contents (Arel & Shaikh, 2018; Frazão et al., 2018; Güneyisi et al., 2013; Guo et al., 2023; Iqbal et al., 2015; Şahmaran et al., 2009; Tang, 2020; Wang et al., 2013; Wei et al., 2020; Wu et al., 2021; Yew et al., 2015; Zhao et al., 2016; Zheng et al., 2019). Non-metallic fibers produced a negligible effect or even decreased compressive strength (Altalabani et al., 2020; Choi et al., 2014; Kayali et al., 2003; Li et al., 2016; Wang et al., 2013) owing to their low stiffness and elastic modulus. PP fibers produced the lowest compressive strength of 46.78 MPa on average, compared with those of PE and carbon fibers (66.79 and 75.34 MPa, respectively). Wei et al. (2020) reported that the PP fibers may have a greater adverse effect on the compressive strength than other fibers at the same volume fraction because of the lower elastic modulus and tensile strength of the PP fiber.

Figure 13 illustrates the compressive strength of L-FRCCs according to the matrix strength. Matrix strength is defined as the compressive strength of the cementitious composites' matrix without fiber reinforcement. As the matrix strength increased, the compressive strength of L-FRCCs increased linearly. In particular, the high-strength matrix (70–100 MPa) of the ULCC resulted in a higher compressive strength (100–150 MPa). In general, the weakest part of L-FRCC is the LWA. Therefore, a higher matrix strength enables L-FRCCs to withstand a greater load even when extreme deformation occurs within the LWAs, resulting in a higher compressive strength (Shafigh et al., 2022; Wang & Wang, 2013).

4.2 Flexural strength

The flexural strength of L-FRCCs ranges between 4.3 and 37.5 MPa, which is acquired from the data in Table 1.

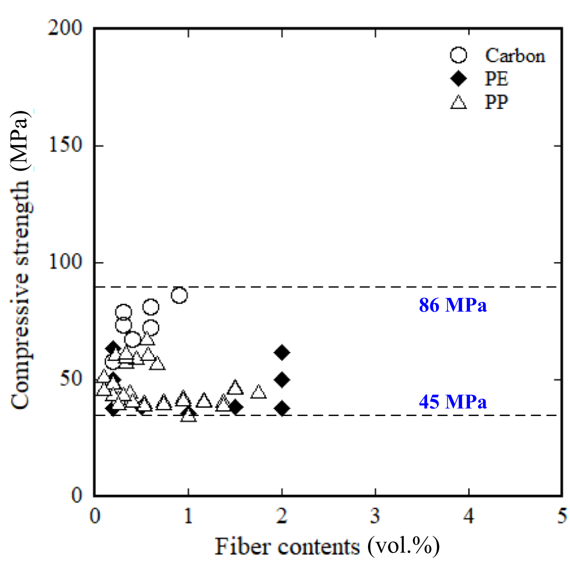

Fig. 12 Effects of non-metallic fiber content on compressive strength

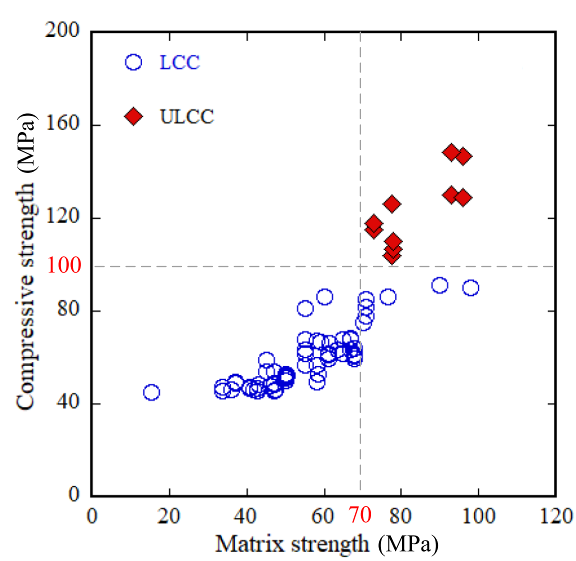

Fig. 13 Effects of matrix strength on compressive strength of L-FRCCs

The flexural strength of L-FRCCs is higher than that of normal concrete (about 4.28 MPa) (Sjah et al., 2018). In general, as the lightweight material content increases, the flexural strength of L-FRCCs decreases owing to the internal voids of lightweight materials, which is similar to the compressive strength results. However, the lightweight material type has no significant influence on the flexural strength because the flexural behavior of L-FRCC is primarily determined by the properties of the fibers (geometry, size, type, and volume content) and the bonding between the fibers and the matrix (Çavdar, 2013; Li et al., 2025; Simões et al., 2017; Zhang et al., 2025).

Figures 14a and b show the flexural strengths of L-FRCCs reinforced with steel and nonmetallic fibers, respectively (Abid et al., 2024; ASTMC, 2017; Balendran et al., 2002; Dawood & Hamad, 2013; Frazão et al., 2018; Gencel et al., 2022; Güneyisi et al., 2013; Hussein et al., 2020; Iqbal et al., 2015; Jiang et al., 2024; Kayali et al., 2003; Liao et al., 2025; Lu et al., 2022b; Mailyan et al., 2021; Mo et al., 2014; Şahmaran et al., 2009; Wu et al., 2019; Xiang et al., 2022; Zeng et al., 2020; Zhang et al., 2024, 2025; Zheng et al., 2025). The flexural strength of the L-FRCCs increased with the volume fraction of steel fibers (Fig. 14a). Several studies have reported that when fibers are reinforced, they resist flexural loads according to the bond between the fibers and the matrix, even after matrix cracking. This further obstructs the crack propagation until the final cracking of the composites and typically results in an overall increase in flexural strength (Balendran et al., 2002; Meng et al., 2023; Rico et al., 2017; Shen et al., 2020a; Xie et al., 2022; Ye et al., 2020; Zhang et al., 2025). Among the various types of steel fibers, straight steel fibers afford higher flexural strength than corrugated and hooked-end steel fibers due to their superior bonding performance. In general, the roughened surface of the fiber produced better bonding with the cement paste (Dawood & Hamad, 2013). However, in the case of high-strength cementitious composites, such as UHPC with a denser matrix, straight steel fibers were more easily dispersed, resulting in better bonding performance between the fibers and matrix (Ye et al., 2020). Straight steel, hooked-end steel, and corrugated steel fibers resulted in average flexural strengths of 14.13, 8.41, and 6.69 MPa, respectively. Ye et al. (2020) reported that L-FRCCs reinforced with micro straight steel fibers showed the highest increase in flexural strength (62%) owing to their superior bonding; hooked-end steel fibers also resulted in a relatively high increase (56%) based on the effective anchorage effect of the hooked-end. However, L-FRCCs reinforced with corrugated steel fibers exhibited only an 11% increase in flexural strength due to the insufficient bonding between the fibers and the matrix.

Although nonmetallic fibers increased the flexural strength of L-FRCCs (Fig. 14b), the degree of increase was considerably smaller than that of metallic fibers.

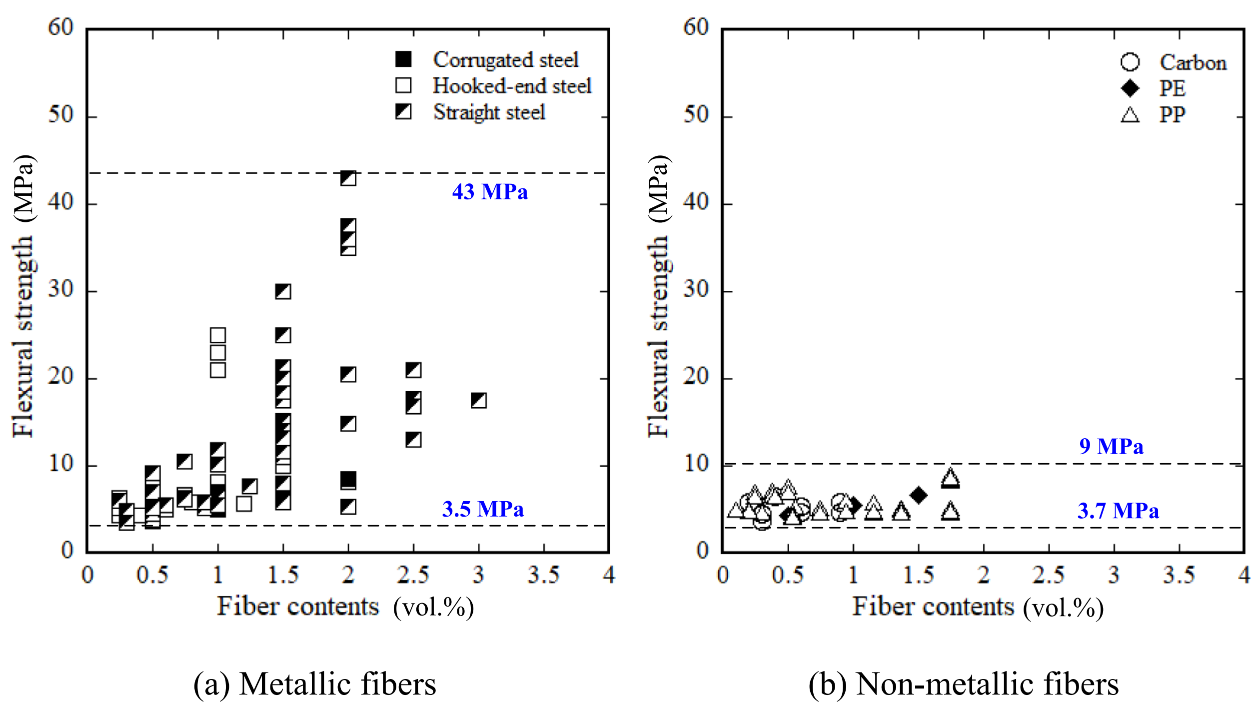

Fig. 14 Effects of fiber content on flexural strength of L-FRCCs

Nonmetallic fibers achieved a flexural strength between 3.7 and 9.0 MPa, whereas metallic fibers achieved between 3.5 and 42.0 MPa. Previous studies on L-FRCCs incorporating polymeric fibers reported that an increase in the volume content of fibers may lead to a decrease in flexural strength or a decrease beyond a certain volume fraction (Kayali et al., 2003; Li et al., 2016; Wei et al., 2020; Yahaghi et al., 2016). Wei et al. (2020) reported that the decrease in flexural strength owing to PP fibers could be attributed to the relatively low elastic moduli. Li et al. (2021a) reported that although fiber reinforcement can restrain crack initiation and propagation under flexural loads, this may significantly reduce the compactness of the cementitious composite matrix. Furthermore, the flexural strength of L-FRCCs with nonmetallic fibers was either minimally affected (Yew et al., 2015) or increased as the aspect ratio of the fibers increased (Altalabani et al., 2020; Li et al., 2021a; Ye et al., 2020). Ye et al. (2020) reported that the low aspect ratio of fibers not only leads to insufficient bonding between the matrix and fibers but also makes it difficult for the fibers to distribute uniformly within the matrix. Further, the high effective surface area, owing to the high aspect ratio of the fibers, was beneficial for enhancing the bond performance between the fiber and cement paste (Li et al., 2021a).

Figure 15 illustrates the flexural strength of L-FRCCs according to the matrix strength. The flexural strength of the L-FRCCs increased significantly as the matrix strength increased. In particular, a high-strength matrix (70–100 MPa) of UHPC produced a higher flexural strength (11–23 MPa) owing to a mechanism similar to that in the compressive strength results.

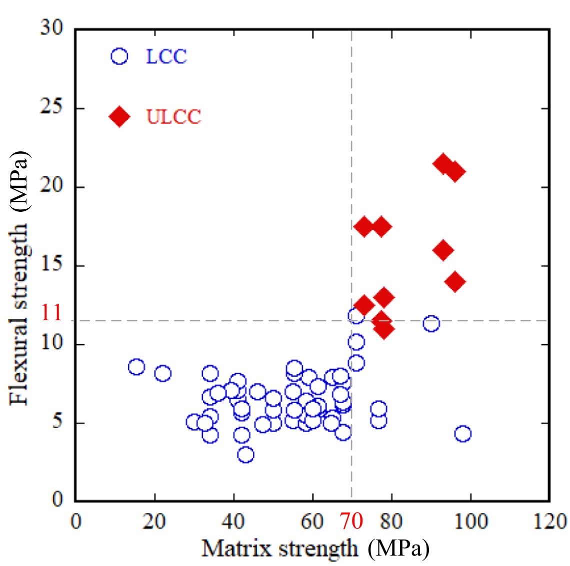

Fig. 15 Effects of matrix strength on flexural strength of L-FRCCs

4.3 Relationship between mechanical properties and density of L-FRCCs

In this section, the relationship between density and the mechanical properties of L-FRCCs—specifically compressive and flexural strength—is examined based on data collected from the literature. Figure 16a illustrates the correlation between compressive strength and density, while Fig. 16b presents the corresponding relationship for flexural strength. As shown in Fig. 16, both compressive and flexural strengths generally increase with increasing density. This trend is expected, as higher density typically reflects a more compact matrix with fewer voids, thereby enhancing mechanical performance. The linear trend lines fitted with the datasets further substantiates this relationship. In Fig. 16a, the coefficient of determination (R^2) indicates that 89.3% of the variability in compressive strength can be attributed to changes in density. The close clustering of data points around the trend line suggests a strong correlation. Although the R^2 value for flexural strength is slightly lower (74.8%), the data points still align closely with the corresponding trend line, demonstrating a robust relationship between density and the flexural strength of L-FRCCs.

5 Structural efficiency of L-FRCCs

SE (strength/density, MPa/(t/m^3)) is a crucial parameter representing the material efficiency of L-FRCCs. A high SE value implies that the L-FRCCs are highly efficient with high strength and low weight (Li et al., 2025; Liao et al., 2025; Lu et al., 2021b). An appropriate selection of lightweight materials and fibers is imperative for producing L-FRCCs with high SE. Lu et al. (2021b) reported three methods to enhance the SE of L-FRCCs: (1) using LWAs with a dense pore structure; (2) increasing the number of surfaces opening pores, thereby increasing the bonding between cement paste and aggregate; and (3) using the internal curing effect of LWA and high pozzolanic reactivity of LWAs.

Figure 17 illustrates the compressive SE of various LWAs, including natural/recycled and artificial LWAs. The compressive SE of L-FRCCs ranges between 17.8 and 66.7 MPa/(t/m^3). Artificial LWAs resulted in a considerably greater SE (within the range 37.6–66.7 MPa/(t/m^3)) than natural or recycled LWAs (17.8–28.1 MPa/(t/m^3)) owing to the inherently higher crushing strength of artificial LWAs than that of natural aggregates. In particular, HGM (Dahal et al., 2022; Guo et al., 2023; Lu et al., 2021a, 2022b) with a high crushing strength of 40–180 MPa and a low average density of 460–560 kg/m^3 resulted in an L-FRCC with the highest SE of 66.7 MPa/(t/m^3). As mentioned in Sect. 4.1, the weakest component in L-FRCCs is the LWA (Shafigh et al., 2022; Wang

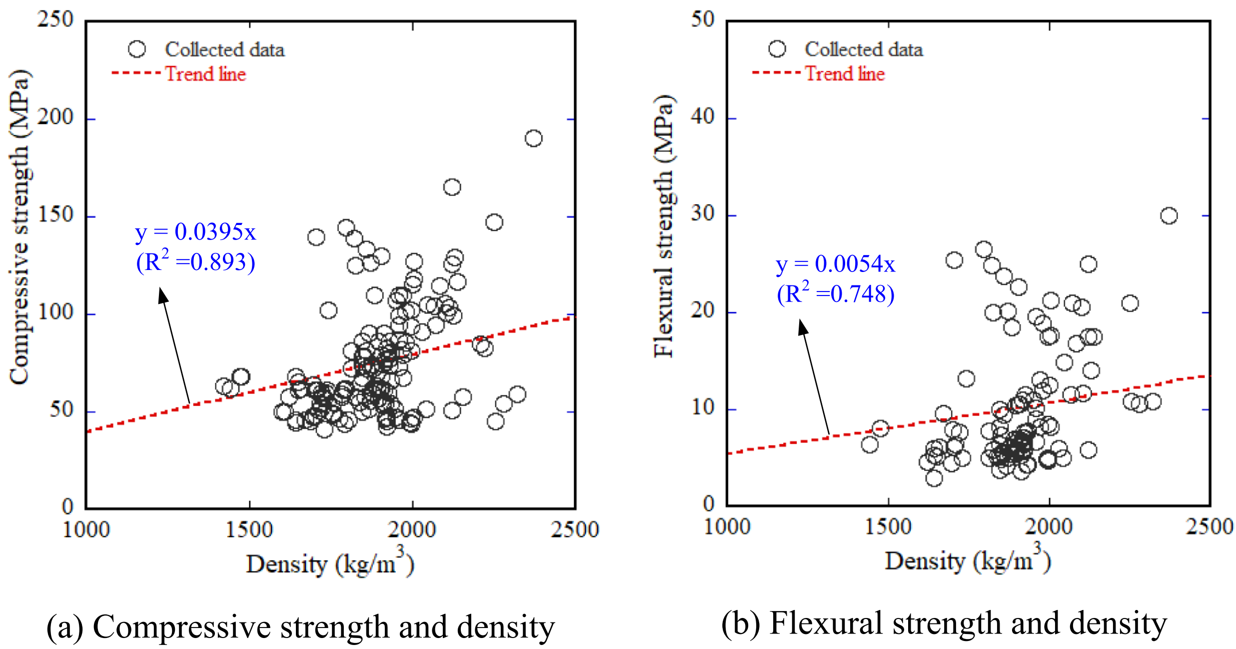

Fig. 16 Correlation between strengths and density of L-FRCCs

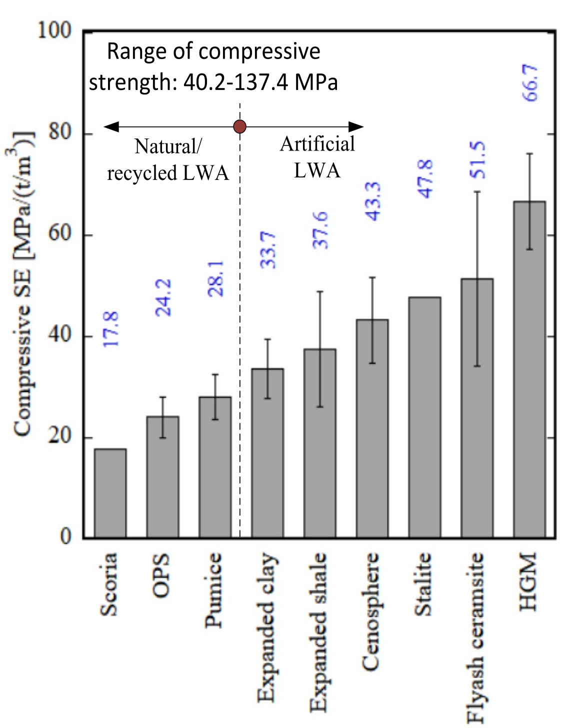

Fig. 17 Effects of LWA types on compressive structural efficiency of L-FRCCs

& Wang, 2013). Therefore, due to the high strength of the LWA, the matrix of L-FRCCs possesses a higher strength.

Table 5 summarizes the available data on the density, compressive strength, and compressive SE of L-LFRCCs, high-strength normal-weight concrete, and other lightweight concretes to better contextualize the material efficiency. Compared to the other five kinds of concrete listed in Table 5, the L-FRCCs prepared with HGMs produced the highest compressive SE, up to 66.7 MPa/(t/m^3), which is 66.7/62.5 = 1.07 times for UHPLCCs (Lu et al., 2021a), 66.7/50 = 1.33 times for UHPC including silica sand (Arora et al., 2019; Wang et al., 2019), 66.7/21.4 = 3.11 times for ultra-lightweight composites (Adhikary et al., 2020; Yu et al., 2015), 66.7/43.5 = 1.53 times for UHPC including LWAs, and 66.7/25 = 2.67 times for high-strength normal-weight concrete (Lu, 2023). It is concluded that the structural efficiency of L-FRCCs prepared with HGMs was better than that of the other cementitious composites.

Figure 18 shows the effects of matrix strength on the compressive SE of L-FRCC. The compressive SE of the L-FRCCs increased with the matrix strength; this trend is similar to the compressive strength results (Sect. 4.1). In particular, the matrix strength and compressive SE exhibited a strong linear relationship with a high coefficient of determination (R^2) of 0.867. Furthermore, L-FRCCs with a high-strength matrix (UHPC) of more than 78 MPa had the highest compressive SE of 48–63 MPa/(t/m^3).

Table 5 Comparison of material efficiency between UL-FRCCs and other FRCCs

Materials	Density (kg/m^3)	Compressive Strength (MPa)	Compressive SE ($MPa/(t/m^3)$)	References
UHPLCCs	< 1920	> 120	62.5	Lu et al. (2021a)
UHPC including silica sand	Normally > 2400	> 120	50.0	Arora et al. (2019), Wang et al. (2019)
Ultra lightweight composites	500 – 1400	5–30	10.0–21.4	Adhikary et al. (2020), Yu et al. (2015)
UHPC including lightweight aggregates	> 2300	> 100	43.5	Meng and Khayat (2017), Liu et al. (2019c)
Normal weight concrete	2400	60	25	Lu (2023)
L-FRCCs	2063.4	139.2	66.7	This study

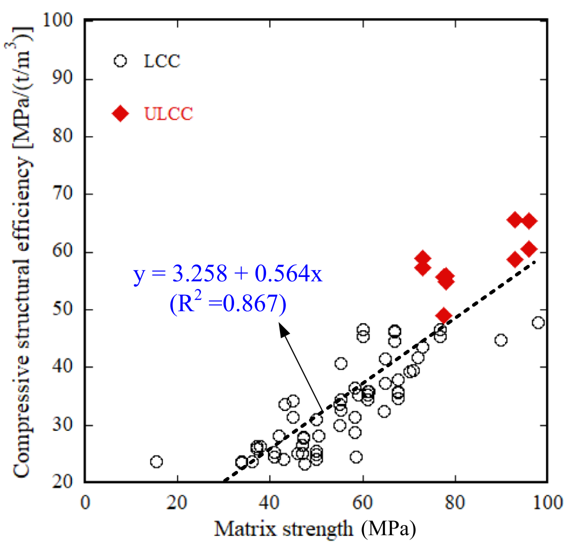

Fig. 18 Effects of matrix strength on compressive structural efficiency

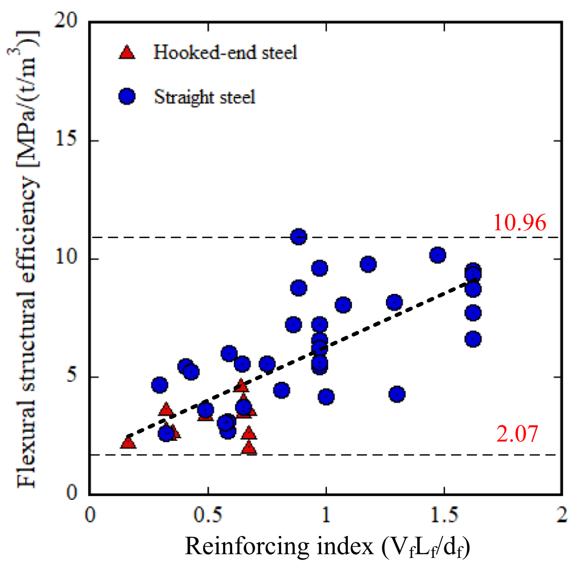

Fig. 19 Effects of reinforcing index of steel fibers on flexural structural efficiency of L-FRCCs

The flexural SE of L-FRCCs ranges between 2.07 and 10.96 $MPa/(t/m^3)$. In general, the flexural SE increases with the volume content of both the steel and PP fibers. The steel fibers resulted in L-FRCCs with a higher flexural SE of 4–9 $MPa/(t/m^3)$ on average than L-FRCC reinforced with PP fibers (3–4.5 $MPa/(t/m^3)$). As mentioned in Sect. 4.2, steel fibers increased the density of L-FRCCs by 6.8% on average, whereas PP fibers decreased it by 2%. Furthermore, owing to the high modulus of elasticity of steel fibers (Wei et al., 2020), steel fibers increased the flexural strength of L-FRCCs by 30.91%, whereas PP fibers increased it by only 5.34%; this trend indicates that a greater increase in flexural strength compared to density may enhance the flexural SE.

Figure 19 shows the effects of the reinforcing index of hooked-end and straight steel fibers on the flexural SE of L-FRCCs. The reinforcing index of fiber ($V_f L_f / d_f$) is defined as a parameter that considers the simultaneous effect of fiber volume content (V_f), length (L_f), and diameter (d_f). The flexural SE of the L-FRCCs increases linearly with the reinforcing index of the steel fibers. As mentioned in Sect. 4.2, the flexural strength of the L-FRCCs decreases with the aspect ratio of the fibers due to their increased effective surface area (Altalabani et al., 2020; Ye et al., 2020). In addition, straight steel fibers exhibited a higher flexural efficiency than hooked-end steel fibers, as indicated by the flexural strength results.

Therefore, to achieve a higher SE of L-FRCC, it is highly recommended to use lightweight materials with a high-strength matrix (> 80 MPa). In addition, utilizing two types of lightweight materials—cement/binder and fine aggregates—can further increase the SE. Furthermore, utilizing straight steel fibers < 2.5% in volume may help achieve a higher SE in the flexural behavior of L-FRCCs.

Figure 20 shows the microstructure of the interfacial transition zone (ITZ) between the mortar and various LWAs, namely fly ash cenospheres (Lu et al., 2022b), HGMs (Lu et al., 2022b), and lightweight high-strength

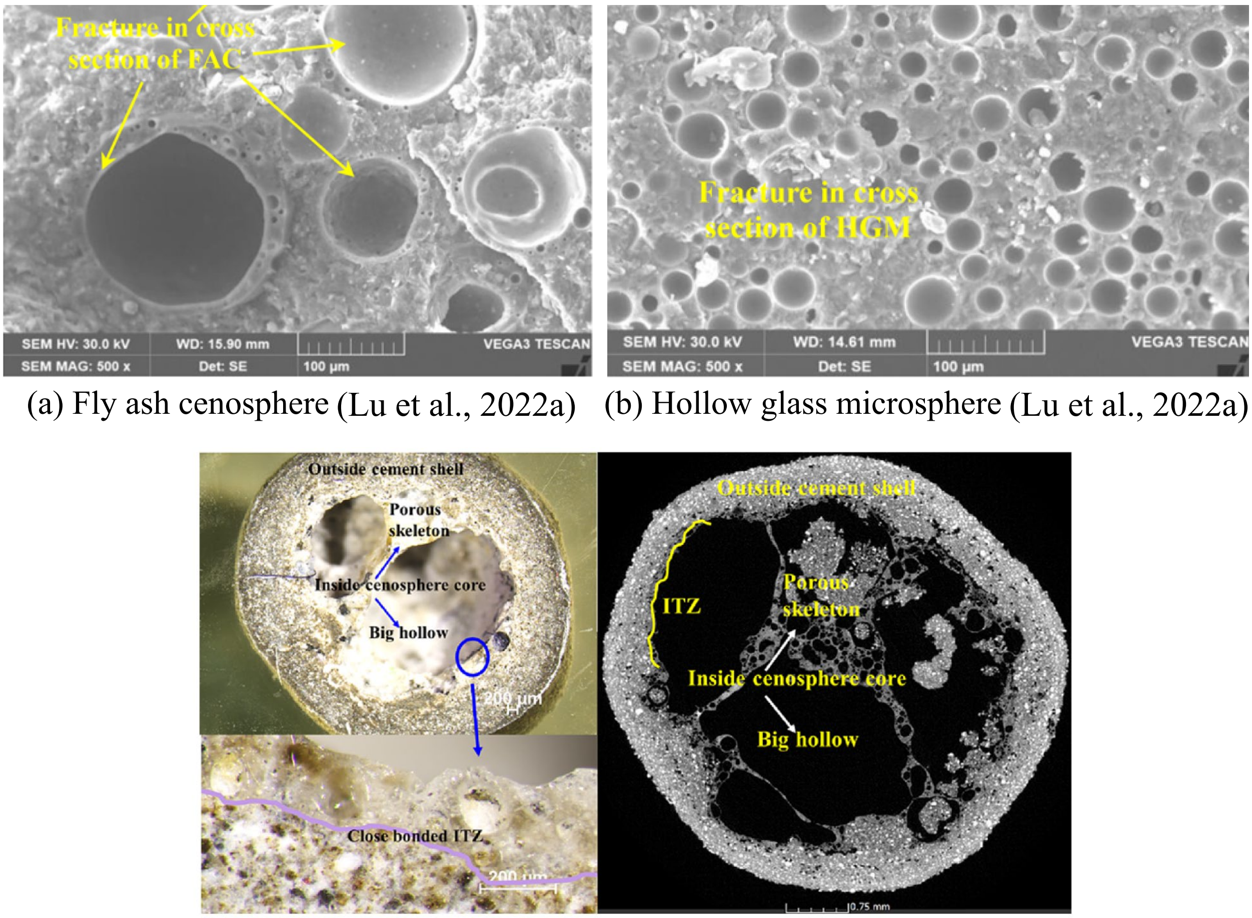

(a) Fly ash cenosphere (Lu et al., 2022a) (b) Hollow glass microsphere (Lu et al., 2022a)

(c) Lightweight high-strength core-shell aggregates (Zou et al., 2023)

Fig. 20 SEM analysis of L-FRCCs

core–shell aggregates (Zou et al., 2023), using scanning electron microscope (SEM). As shown in Fig. 20a, when fly ash cenospheres were added to the matrix-based UHPC, the HGMs were seen as embedded in the matrix. Under applied load, the cross-sections of the fly ash cenospheres were damaged, indicating their brittle behavior, while the bond between the fly ash cenospheres and the matrix remained strong. In the case of HGMs, some HGMs fractured internally, while others failed at the interface with the paste (Fig. 20b), indicating that a larger portion of HGMs could withstand the loading stress compared to fly ash cenospheres. This behavior can be attributed to the smoother surface of HGMs, which results in a weaker bond with the surrounding matrix (Duy et al., 2026).

Several approaches have been proposed in recent years to achieve the ultra-high strength of ULCCs. One notable method involves the development of high-strength lightweight core–shell aggregates (Tajra et al., 2019; Zou et al., 2023). In this technique, traditional LWAs (e.g., cenospheres) serve as the core material, which is subsequently coated with a hard-shell layer, typically composed of hydrated cement paste (Zou et al., 2023), as illustrated in Fig. 20c.

6 Pearson's correlation analysis

To assess the statistical relationship between input parameters (fiber volume content, reinforcing index, and LWA ratio), the material properties (slump and density), as well as the mechanical properties (compressive strength, flexural strength, compressive structural efficiency, and flexural structural efficiency) of L-FRCCs, the Pearson correlation coefficient was employed (Li et al., 2021b; Phan et al., 2025). The mathematical function used to compute Pearson's correlation coefficient is provided below:

$$p(A,B) = \frac{\sum \left(A_i - \bar{A}\right) \sum \left(B_i - \bar{B}\right)}{\sqrt{\sum \left(A_i - \bar{A}\right)^2 \sum \left(B_i - \bar{B}\right)^2}} \quad (1)$$

Here, p represents the Pearson correlation coefficient. The p value ranges from − 1.0 to + 1.0, where 0.0 signifies no correlation between the two parameters, + 1.0 indicates a perfect direct correlation, and − 1.0 denotes a perfect inverse correlation. A and B are the two parameters under investigation, while $\overline{A}$ and $\overline{B}$ denote their respective averaged values.

Among the material property parameters, there is limited information on thermal conductivity is limited; therefore, it was difficult to consider this parameter in the Pearson correlation analysis. Figure 21 illustrates correlation matrices depicting the relationships among the design parameters influencing material properties, such as slump and density, and mechanical properties, including the compressive strength, flexural strength, compressive SE, and flexural SE of L-FRCCs. According to Fig. 21, the slump of L-FRCCs exhibited a low inverse correlation with the reinforcing index and LWA ratio, with Pearson correlation coefficients of − 0.028 and − 0.15, respectively; this indicates that the slump decreased as the reinforcing index and LWA ratio increased. Conversely, there was a direct correlation between slump and density, compressive strength, flexural strength, compressive SE, and flexural SE, with a Pearson correlation coefficient of 0.27, 0.29, 0.22, 0.30, and 0.16, respectively.

The density of L-FRCCs shows a strong negative correlation with the LWA ratio, with Pearson correlation coefficients of − 0.21; this indicates that the density decreases when the LWA ratio increases. Conversely, the density of L-FRCCs exhibits a positive correlation with compressive strength, flexural strength, compressive SE, flexural SE, matrix strength, and fiber volume content, with Pearson correlation coefficients of 0.41, 0.38, 0.18, 0.24, 0.19, and 0.19, respectively.

Further, the compressive strength, flexural strength, compressive SE, flexural SE, and matrix strength of L-FRCCs demonstrate a significant negative correlation with the LWA ratio, with Pearson correlation coefficients of − 0.38, − 0.63, − 0.48, − 0.54, and − 0.29, respectively. These results indicate that lower values of these

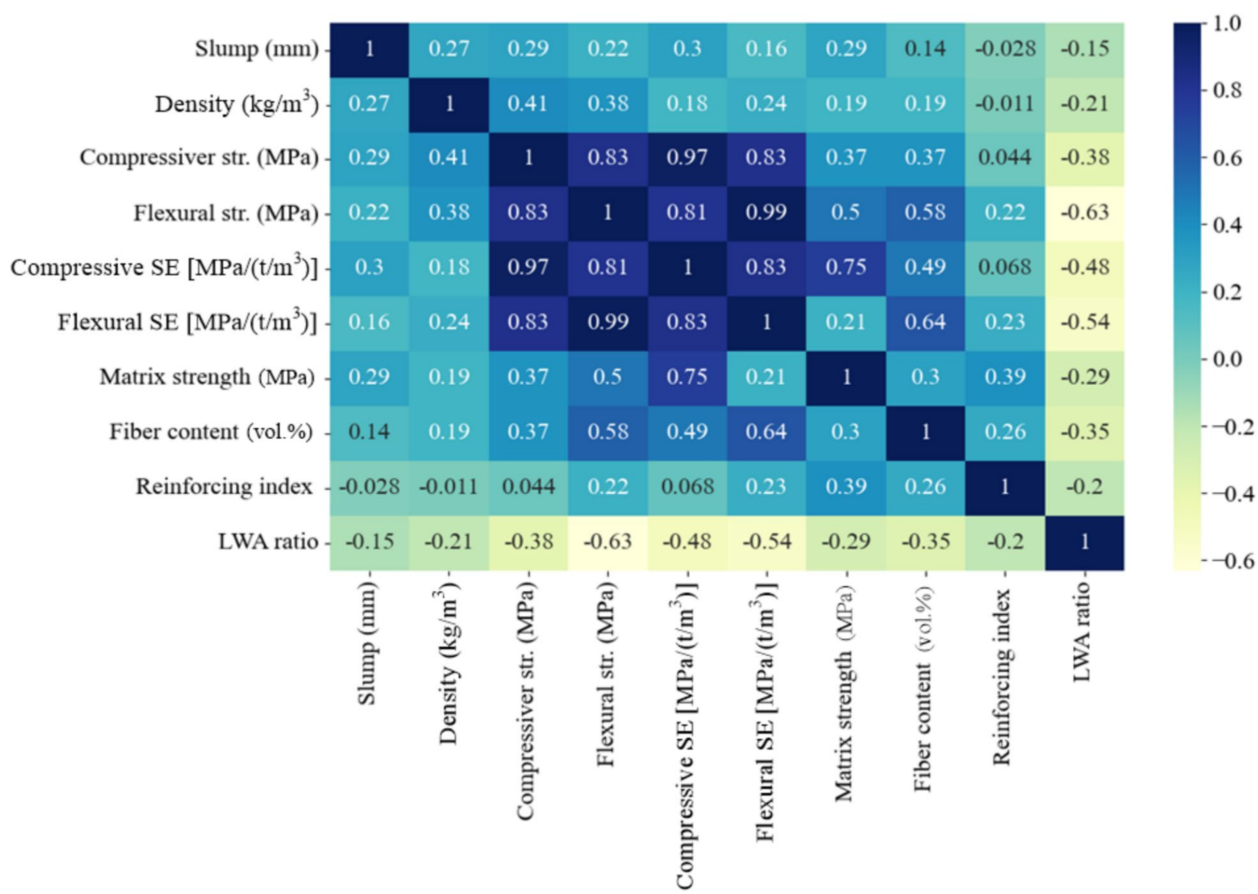

Fig. 21 Pearson's correlation coefficients among design parameters related to material and mechanical properties of L-FRCCs

parameters are associated with an increasing LWA ratio in L-FRCCs.

Significant positive correlations were found between compressive strength, flexural strength, flexural SE, matrix strength, fiber volume content, and compressive SE, with Pearson correlation coefficients of 0.97, 0.81, 0.83, 0.75, and 0.49, respectively. Similarly, there are notably high positive correlation between compressive strength, flexural strength, matrix strength, fiber volume content, and flexural SE, with Pearson correlation coefficients of 0.83, 0.99, 0.21, and 0.64, respectively. These findings suggest that the compressive and flexural SE of L-FRCCs increased with increasing compressive and flexural strengths, matrix strength, and fiber volume content.

7 Application

Lightweight cementitious composites, exhibiting significantly lower density than conventional cementitious composites due to a higher proportion of pores, have gained significant attention for use as an alternative construction material capable of reducing the structural load and have been used extensively. Lightweight cementitious composites have been successfully applied in high-rise buildings, such as the 180-m towers in Chicago (1947), North Pier Apartment Tower in Chicago (1990), and the tower of the Bank of America (1997) The tower of the Bank of America was built using lightweight cementitious composites with a density lower than 1890 kg/m^3 and a compressive strength greater than 45 MPa (Abdalla, 2007). Lightweight cementitious composites have been used in bridges, such as Kingston Bridge in London (1997) and Stolma Bridge in Norway (2000), and in large-span public structures, such as Terminal 3 Concourse in Dubai International Airport (2010) (Farrag & Yehia, 2014) and Wellington Westpac Trust Stadium in New Zealand (1999). Furthermore, the lightweight cementitious composites have been used for marine structures such as Modular Hybrid Pier floats for Navy in USA and in the Wreck of the San Pasqual—a lightweight concrete ship in USA (1991). Figure 22 presents photograph of these structures that utilize lightweight cementitious composites, and Table 6 provides detailed information on the properties of these structures. The application of lightweight cementitious composites in these structures indicate that, with the increasing feasibility of constructing large-scale structures, the weight of concrete has gradually become as crucial as its strength (Meng et al., 2023).

However, to address various drawbacks such as the low tensile–compressive strength ratio, low flexural strength, and high brittleness of lightweight cementitious composites (Wang & Wang, 2013), extensive research has been conducted to develop high-strength lightweight cementitious composites by reinforcing them with fibers. When reinforced with fibers, both lightweight and conventional cementitious composites exhibit significantly enhanced energy absorption capacities, leading to higher flexural and tensile strengths and increased impact resistance. Thus, the structural behavior of L-FRCCs against seismic forces has improved, rendering them suitable for use in earthquake-prone regions (Rico et al., 2017). Furthermore, in recent times, LWAs have been incorporated in UHP-FRCCs owing to their superior strength, ductility, and durability compared to conventional fiber-reinforced concrete. These UHP-FRCCs exhibit strain-hardening behavior under tensile loading, exceptional tensile strength, ductility, high strain capacity, and outstanding energy absorption, providing remarkable resistance against high impacts. However, despite these advantages, they possess drawbacks such as relatively high shrinkage and high density owing to the low water-to-cement ratio and high packing density (Meng et al., 2023). The internal curing effect and notable lightweight properties of LWAs have been recognized to mitigate self-shrinkage (Ahmaran et al., 2015; Şahmaran et al., 2009) and thus reduce the density of UHP-FRCCs. Moreover, some other disadvantages of UL-FRCCs include higher material cost resulting from the use of fine powders, fibers, and chemical admixtures; complex mixing and procedures, which can affect their workability and uniform fiber dispersion; and potential brittleness under restrained shrinkage or improper curing conditions, leading to early-age cracking.

Consequently, incorporating LWAs in UHP-FRCCs enabled the production of UL-FRCCs with compression strengths > 100 MPa and flexural strengths > 15 MPa. However, the application of UL-FRCCs to real construction sites has not been reported as most studies have been limited to analyzing the effects of lightweight materials on the material properties and static strength of UL-FRCCs. Therefore, expanding the analysis to encompass not only static behavior but also dynamic behaviors, such as impact strength, may enable a wider range of applications of UL-FRCCs. Moreover, there is a need for detailed experimental studies focusing on the optimal contents for lightweight materials and fibers, in addition to the microstructure and functional properties, such as sound absorption.

Consequently, UL-FRCCs are anticipated to find applications not only in large-scale structures, such as long-span bridges and high-rise buildings, but also in barriers and protective structures situated in regions prone to high and repeated impact loads, such as vehicle and ship collisions, rock falls, missile impacts, explosions, and earthquakes.

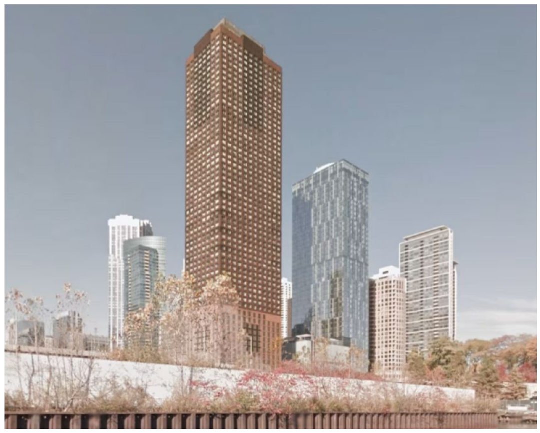

a) North Pier Apartment Tower, Chicago

(Figure sourced from https://buildingsdb.com/IL/chicago/north-pier-apartments-building/.)

b) Kingston Bridge, England

(Figure sourced from https://commons.wikimedia.org/wiki)

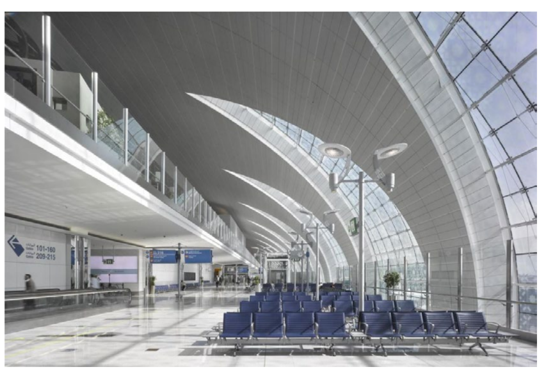

c) Dubai International Terminal 3, United Arab Emirates

(Figure sourced from https://www.matteograssi.com/en/projects/dubai-airport)

Fig. 22 Images of real structures constructed using L-FRCCs

8 Summary and conclusions

This study summarizes the material and mechanical properties of existing high-strength L-FRCCs with compressive strengths > 45 MPa, focusing on further enhancing the SE of L-FRCCs. First, the effects of different fibers, LWAs, and matrix strengths on the material

d) Wellington Westpac Trust Stadium, New Zealand

(Figure sourced from https://www.cricwindow.com/icc-worldcup-2015/westpac-match-schedule.html.)

e) Modular Hybrid Pier (MHP) floats for Navy, USA

(Figure sourced from https://www.concretetech.com/concrete-projects/modular-hybrid-pier.)

Fig. 22 continued

Table 6 Properties of structures using lightweight concrete in practical projects

Application	Project	Structural component	Unit weight (kg/m^3)	Compressive strength at 28 days (MPa)	Lightweight material used
Buildings	North Pier Apartment Tower, Chicago	Floor slabs	–	44.0	–
	Bank of America, USA	Floor slabs	1890	47.0	Expanded shale
Bridges	Stolma Bridge, Norway	Mid-span cantilevers	1940	70.4	Expanded clay
Large-span public structures	Dubai International Terminal 3, United Arab Emirates	Mezzanine levels	1900	50.0	–
	Wellington Westpac Trust Stadium, New Zealand	Stadium bowl structure, Pretensioned bleachers	1845	44.0	Expanded shale
Marine structures	Wreck of the San Pasqual: lightweight concrete ship, USA	Lightweight concrete ship	1760	55.0	Expanded shale

and mechanical properties of L-FRCCs were analyzed. The material properties included workability, density, and thermal conductivity, whereas the mechanical properties included compressive strength, flexural strength, and structural efficiency. Based on the analysis of the currently available experimental results, the following conclusions were drawn:

- L-FRCCs with a compressive strength > 100 MPa, flexural strength > 15 MPa, density < 1950 kg/m^3, and thermal conductivity < 0.5 W/mK can be classified as UL-FRCCs.

- Incorporating HGM into L-FRCCs substantially enhanced their sound absorption performance, which is attributed to the formation of numerous acoustic cavities.
- Based on the Pearson correlation analysis, the SE in terms of the strength of L-FRCCs increased with increasing matrix strength, fiber volume content, and reinforcing index, while it decreased with a higher LWA ratio.
- To produce UL-FRCCs with high SE, the lightweight materials incorporated in the UL-FRCCs should have crushing strength > 70 MPa but specific gravity < 0.5. Utilizing straight steel fibers at < 2.5 vol.% in UL-FRCCs is highly recommended to achieve a high strength of more than 100 MPa.
- Steel fibers reduced the workability of the L-FRCCs owing to their inherently high stiffness compared with other nonmetallic fibers, such as polymeric fibers. However, steel fibers resulted in a higher SE with flexural strength than polymeric fibers.

Abbreviations

ACI	American Concrete Institute
CCS	Cloud concrete stone
CNT	Carbon nanotube
ECLA	Expanded clay lightweight aggregate
ESLA	Expanded shale lightweight aggregate
FCLA	Fly ash cenosphere lightweight aggregate
HGMs	Hollow glass microspheres
LCC	Lightweight cementitious composite
L-FRCCs	Lightweight fiber-reinforced cementitious composites
LWA	Lightweight aggregate
LWC	Lightweight concrete
OPS	Oil palm shell
PE	Polyethylene
PP	Polypropylene
PVA	Polyvinyl Alcohol
RPC	Reactive powder concrete
SE	Structural efficiency
SFLA	Sintered fly ash lightweight aggregate
UHPC	Ultra-high-performance concrete
UHSLC	Ultra-high-strength lightweight concrete
ULCC	Ultra-high-performance lightweight cementitious composite
UL-FRCCs	Ultra-high-strength lightweight fiber-reinforced cementitious composites
UHP-FRCCs	Ultra-high-performance fiber-reinforced cementitious composites

Author contributions

SSJ: Writing–original draft, Visualization, Validation, Software, Methodology, Investigation. TDP: Writing–original draft, Visualization, Validation, Software, Methodology, Investigation. DHL: Writing–review & editing, Resources. SYC: Writing–review & editing, Methodology. DJK: Writing–review & editing, Supervision, Resources, Project administration, Funding acquisition.

Funding

This work was supported by the National Research Foundation of Korea (NRF) grant funded by the Korean Government (MSIT) (No. 2022R1A2C2005234).

Availability of data and materials

The datasets used and/or analyzed during the current study are available from the corresponding author on reasonable request.

Declarations

Competing interests

The authors declare that they have no known competing financial interests or personal relationships that could have appeared to influence the work reported in this paper.

Received: 8 September 2025 Accepted: 10 December 2025
Published online: 03 January 2026

References

Abdalla, M. (2007). High-performance lightweight concrete. www.escsi.org.

Abid, M., Waqar, G. Q., Mao, J., Javed, M. F., & Almujibah, H. (2024). Mechanical properties, microstructure and GEP-based modeling of basalt fiber reinforced lightweight high-strength concrete containing SCMs. *Journal of Building Engineering, 96*, Article 110378. https://doi.org/10.1016/j.jobe.2024.110378

Adhikary, S. K., Rudžionis, Ž, & Vaičiukynienė, D. (2020). Development of flowable ultra-lightweight concrete using expanded glass aggregate, silica aerogel, and prefabricated plastic bubbles. *Journal of Building Engineering, 31*, Article 101399. https://doi.org/10.1016/j.jobe.2020.101399

Ahmaran, M. S., Yildirim, G., Al-Emam, M. K. M., Hameed, R. K. H., Al-Najjar, Y., & Lachemi, M. (2015). Effects of compressive strength, autogenous shrinkage and testing methods on the bond behavior of HES-ECC. *ACI Materials Journal*. https://doi.org/10.14359/51687188

Alanazi, H., Elalaoui, O., Adamu, M., Alaswad, S. O., Ibrahim, Y. E., Abadel, A. A., & Al Fuhaid, A. F. (2022). Mechanical and microstructural properties of ultra-high performance concrete with lightweight aggregates. *Buildings, 12*, 1–13. https://doi.org/10.3390/buildings12111783

Altalabani, D., Bzeni, D. K. H., & Linsel, S. (2020). Mechanical properties and load deflection relationship of polypropylene fiber reinforced self-compacting lightweight concrete. *Construction and Building Materials, 252*, Article 119084. https://doi.org/10.1016/j.conbuildmat.2020.119084

Arel, H. Ş, & Shaikh, F. U. A. (2018). Effects of silica fume fineness on mechanical properties of steel fiber reinforced lightweight concretes subjected to ambient and elevated temperatures exposure. *Structural Concrete, 19*, 1829–1837. https://doi.org/10.1002/suco.201700281

Arenas, C., Leiva, C., Vilches, L. F., & Cifuentes, H. (2013). Use of co-combustion bottom ash to design an acoustic absorbing material for highway noise barriers. *Waste Management, 33*, 2316–2321. https://doi.org/10.1016/j.wasman.2013.07.008

Arora, A., Almujaddidi, A., Kianmofrad, F., Mobasher, B., & Neithalath, N. (2019). Material design of economical ultra-high performance concrete (UHPC) and evaluation of their properties. *Cement and Concrete Composites, 104*, Article 103346. https://doi.org/10.1016/j.cemconcomp.2019.103346

Aslani, F., Sun, J., Bromley, D., & Ma, G. (2019). Fiber-reinforced lightweight self-compacting concrete incorporating scoria aggregates at elevated temperatures. *Structural Concrete, 20*, 1022–1035. https://doi.org/10.1002/suco.201800231

ASTMC1856 (2017). Standard Practice for fabricating and testing specimens of ultra- high performance concrete, ASTM Int. West Conshohocken, PA, USA

Balendran, R. V., Zhou, F. P., Nadeem, A., & Leung, A. Y. T. (2002). Influence of steel fibres on strength and ductility of normal and lightweight high strength concrete. *Building and Environment, 37*, 1361–1367. https://doi.org/10.1016/S0360-1323(01)00109-3

Caratelli, A., Imperatore, S., Meda, A., & Rinaldi, Z. (2016). Punching shear behavior of lightweight fiber reinforced concrete slabs. *Composites Part B: Engineering, 99*, 257–265. https://doi.org/10.1016/j.compositesb.2016.06.045

Carbajo, J., Esquerdo-Lloret, T. V., Ramis, J., Nadal-Gisbert, A. V., & Denia, F. D. (2015a). Acoustic properties of porous concrete made from arlite and

vermiculite lightweight aggregates. *Materiales De Construcción*. https://doi.org/10.3989/mc.2015.01115
Carbajo, J., Ramis, J., Godinho, L., Amado-Mendes, P., & Alba, J. (2015b). A finite element model of perforated panel absorbers including viscothermal effects. *Applied Acoustics, 90*, 1–8. https://doi.org/10.1016/j.apacoust.2014.10.013
Çavdar, A. (2013). The effects of high temperature on mechanical properties of cementitious composites reinforced with polymeric fibers. *Composites Part B: Engineering, 45*, 78–88. https://doi.org/10.1016/j.compositesb.2012.09.033
Chen, B., & Liu, J. (2005). Contribution of hybrid fibers on the properties of the high-strength lightweight concrete having good workability. *Cement and Concrete Research, 35*, 913–917. https://doi.org/10.1016/j.cemconres.2004.07.035
Chiadighikaobi, P. C. (2019). Effects of basalt fiber in lightweight expanded clay concrete on compressive strength and flexural strength of lightweight basalt fiber reinforced concrete. *IOP Conference Series Materials Science and Engineering*. https://doi.org/10.1088/1757-899X/640/1/012055
Choi, J., Zi, G., Hino, S., Yamaguchi, K., & Kim, S. (2014). Influence of fiber reinforcement on strength and toughness of all-lightweight concrete. *Construction and Building Materials, 69*, 381–389. https://doi.org/10.1016/j.conbuildmat.2014.07.074
ACI Committee 363.2R-10 (2010) Report on high-strength, concrete communications, American Concrete Institute.
ACI Committee 213R-14 (2014). Guide for structural lightweight-aggregate concrete.
Dahal, M., Liyew, G., Kim, H. K., & Pyo, S. (2022). Characteristics of ultra-high performance lightweight concrete containing hollow glass microspheres under severe loading conditions. *Construction and Building Materials, 356*, Article 129312. https://doi.org/10.1016/j.conbuildmat.2022.129312
Dawood, E. T., & Hamad, A. J. (2013). High performance lightweight concrete reinforced with glass fibers. *AL-Mansour Journal*. https://doi.org/10.36541/0231-000-020-015
Duy, T., Sung, S., & Joo, D. (2026). Tensile response of ultra-high performance lightweight fiber-reinforced cementitious composite containing hollow glass microspheres at high strain rates. *Cement and Concrete Composites, 166*, Article 106390. https://doi.org/10.1016/j.cemconcomp.2025.106390
BS EN 1992-1-1 (2004). Eurocode 2: Design of concrete structures: part 1-1: General rules and rules for buildings, Br. Stand. Institution, London
Esmaeili, J., Ghaffarinia, M., Nodehi, M., Gencel, O., Shi, J., & Ozbakkaloglu, T. (2023). Mechanical and fractural characteristics of structural lightweight fiber reinforced concrete. *Structural Concrete, 24*, 2420–2439. https://doi.org/10.1002/suco.202200107
Farrag, S., & Yehia, S. (2014). Impact of mix preparation on strength and workability of high strength self-consolidated lightweight concrete. *IOSR Journal of Mechanical and Civil Engineering, 11*, 58–69. https://doi.org/10.9790/1684-11455869
Frazão, C., Barros, J., Toledo Filho, R., Ferreira, S., & Gonçalves, D. (2018). Development of sandwich panels combining Sisal Fiber-Cement Composites and Fiber-Reinforced Lightweight Concrete. *Cement and Concrete Composites, 86*, 206–223. https://doi.org/10.1016/j.cemconcomp.2017.11.008
Gao, J., Sun, W., & Morino, K. (1997). Mechanical properties of steel fiber-reinforced, high-strength, lightweight concrete. *Cement and Concrete Composites, 19*, 307–313. https://doi.org/10.1016/S0958-9465(97)00023-1
Gencel, O., Nodehi, M., Bayraktar, O. Y., Kaplan, G., Benli, A., Gholampour, A., & Ozbakkaloglu, T. (2022). Basalt fiber-reinforced foam concrete containing silica fume: An experimental study. *Construction and Building Materials, 326*, Article 126861. https://doi.org/10.1016/j.conbuildmat.2022.126861
Gondokusumo, G. S., Venkateshwaran, A., Tan, K. H., & Liew, J. Y. R. (2021). Unified equations to predict residual flexural tensile strength of lightweight steel fiber-reinforced concrete. *Structural Concrete, 22*, 2202–2222. https://doi.org/10.1002/suco.202100172
Güneyisi, E., Gesoǧlu, M., & Ipek, S. (2013). Effect of steel fiber addition and aspect ratio on bond strength of cold-bonded fly ash lightweight aggregate concretes. *Construction and Building Materials, 47*, 358–365. https://doi.org/10.1016/j.conbuildmat.2013.05.059
Guo, P., Meng, W., Du, J., Han, B., & Bao, Y. (2023). Lightweight ultra-high-performance concrete (UHPC) with expanded glass aggregate: Development, characterization, and life-cycle assessment. *Construction & Building Materials, 371*, Article 130441. https://doi.org/10.1016/j.conbuildmat.2023.130441
Hassanpour, M., Shafigh, P., & Mahmud, H. B. (2012). Lightweight aggregate concrete fiber reinforcement—A review. *Construction and Building Materials, 37*, 452–461. https://doi.org/10.1016/j.conbuildmat.2012.07.071
Hong, S. H., Choi, J. S., Lee, H. J., & Yoon, Y. S. (2025). Thermal and sound insulation characteristics of CNT infused ultra-high-strength lightweight concrete (UHSLC). *Cement and Concrete Composites, 164*, Article 106221. https://doi.org/10.1016/j.cemconcomp.2025.106221
Hosen, M. A., Shammas, M. I., Shill, S. K., Al-Deen, S., Jumaat, M. Z., & Hashim, H. (2022). Ductility enhancement of sustainable fibrous-reinforced high-strength lightweight concrete. *Polymers*. https://doi.org/10.3390/polym14040727
Hossain, K. M. A. (2004). Properties of volcanic scoria based lightweight concrete. *Magazine of Concrete Research, 56*, 111–120. https://doi.org/10.1680/macr.2004.56.2.111
Hussein, Z. M., Khalil, W. I., & Ahmed, H. K. (2020). Shrinkage and impact strength of fibre-reinforced artificial lightweight aggregate concrete. *IOP Conference Series Materials Science and Engineering*. https://doi.org/10.1088/1757-899X/671/1/012118
Iqbal, S., Ali, A., Holschemacher, K., & Bier, T. A. (2015). Mechanical properties of steel fiber reinforced high strength lightweight self-compacting concrete (SHLSCC). *Construction and Building Materials, 98*, 325–333. https://doi.org/10.1016/j.conbuildmat.2015.08.112
Jiang, F., Deng, W., Wang, Q., Wang, J., & Mao, Z. (2024). Performance research and engineering application of fiber-reinforced lightweight aggregate concrete. *Materials*. https://doi.org/10.3390/ma17225530
Johnson Alengaram, U., Al Muhit, B. A., bin Jumaat, M. Z., & Jing, M. L. Y. (2013). A comparison of the thermal conductivity of oil palm shell foamed concrete with conventional materials. *Materials & Design, 51*, 522–529. https://doi.org/10.1016/j.matdes.2013.04.078
Kayali, O., Haque, M. N., & Zhu, B. (2003). Some characteristics of high strength fiber reinforced lightweight aggregate concrete. *Cement and Concrete Composites, 25*, 207–213. https://doi.org/10.1016/S0958-9465(02)00016-1
Kim, H. K., & Lee, H. K. (2010). Influence of cement flow and aggregate type on the mechanical and acoustic characteristics of porous concrete. *Applied Acoustics, 71*, 607–615. https://doi.org/10.1016/j.apacoust.2010.02.001
Li, H., Wei, Y., Zhao, L., Hu, S., Zhu, B., & Ye, P. (2025). Experimental and theoretical studies on fracture performance of bamboo fiber-reinforced lightweight aggregate concrete. *Construction and Building Materials, 465*, Article 140250. https://doi.org/10.1016/j.conbuildmat.2025.140250
Li, J. J., Niu, J. G., Wan, C. J., Jin, B., & Yin, Y. L. (2016). Investigation on mechanical properties and microstructure of high performance polypropylene fiber reinforced lightweight aggregate concrete. *Construction and Building Materials, 118*, 27–35. https://doi.org/10.1016/j.conbuildmat.2016.04.116
Li, J., Zhao, E., Niu, J., & Wan, C. (2021a). Study on mixture design method and mechanical properties of steel fiber reinforced self-compacting lightweight aggregate concrete. *Construction and Building Materials, 267*, Article 121019. https://doi.org/10.1016/j.conbuildmat.2020.121019
Li, Y., Zhang, G., Yang, J., Ding, Y., Ding, Q., & Wang, Y. (2022). Chloride ion transport properties in lightweight ultra-high-performance concrete with different lightweight aggregate particle sizes. *Materials*. https://doi.org/10.3390/ma15196626
Li, Z., Gao, X., & Lu, D. (2021b). Correlation analysis and statistical assessment of early hydration characteristics and compressive strength for multi-composite cement paste. *Construction and Building Materials, 310*, Article 125260. https://doi.org/10.1016/j.conbuildmat.2021.125260
Liao, Q., Lu, S. Y., Lu, J. X., & Poon, C. S. (2025). Improving mechanical and fracture properties of high-performance lightweight concrete by using steel fiber and sustainable high-strength core-shell lightweight aggregate. *Construction and Building Materials, 459*, Article 139697. https://doi.org/10.1016/j.conbuildmat.2024.139697
Ling, T. C., Nor, H. M., & Lim, S. K. (2010). Using recycled waste tyres in concrete paving blocks. *Proceedings of the Institution of Civil Engineers. Waste and Resource Management, 163*, 37–45. https://doi.org/10.1680/warm.2010.163.1.37

Liu, H., Elchalakani, M., Karrech, A., Yehia, S., & Yang, B. (2021). High strength flowable lightweight concrete incorporating low C3A cement, silica fume, stalite and macro-polyfelin polymer fibres. *Construction and Building Materials, 281*, Article 122410. https://doi.org/10.1016/j.conbuildmat.2021.122410
Liu, J., Shi, C., Farzadnia, N., & Ma, X. (2019c). Effects of pretreated fine lightweight aggregate on shrinkage and pore structure of ultra-high strength concrete. *Construction and Building Materials, 204*, 276–287. https://doi.org/10.1016/j.conbuildmat.2019.01.205
Liu, K., Yu, R., Shui, Z., Li, X., Guo, C., Yu, B., & Wu, S. (2019a). Optimization of autogenous shrinkage and microstructure for Ultra-High Performance Concrete (UHPC) based on appropriate application of porous pumice. *Construction and Building Materials, 214*, 369–381. https://doi.org/10.1016/j.conbuildmat.2019.04.089
Liu, X., Wu, T., & Liu, Y. (2019b). Stress-strain relationship for plain and fibre-reinforced lightweight aggregate concrete. *Construction and Building Materials, 225*, 256–272. https://doi.org/10.1016/j.conbuildmat.2019.07.135
Lu, J. X. (2023). Recent advances in high strength lightweight concrete: From development strategies to practical applications. *Construction and Building Materials, 400*, Article 132905. https://doi.org/10.1016/j.conbuildmat.2023.132905
Lu, J. X., Ali, H. A., Jiang, Y., Guan, X., Shen, P., Chen, P., & Poon, C. S. (2022b). A novel high-performance lightweight concrete prepared with glass-UHPC and lightweight microspheres: Towards energy conservation in buildings. *Composites Part B: Engineering, 247*, Article 110295. https://doi.org/10.1016/j.compositesb.2022.110295
Lu, J. X., Shen, P., Ali, H. A., & Poon, C. S. (2021b). Development of high performance lightweight concrete using ultra high performance cementitious composite and different lightweight aggregates. *Cement and Concrete Composites, 124*, Article 104277. https://doi.org/10.1016/j.cemconcomp.2021.104277
Lu, J. X., Shen, P., Sun, Y., & Poon, C. S. (2022a). Strategy for preventing explosive spalling and enhancing material efficiency of lightweight ultra high-performance concrete. *Cement and Concrete Research, 158*, Article 106842. https://doi.org/10.1016/j.cemconres.2022.106842
Lu, J. X., Shen, P., Zheng, H., Ali, H. A., & Poon, C. S. (2021a). Development and characteristics of ultra high-performance lightweight cementitious composites (UHP-LCCs). *Cement and Concrete Research, 145*, Article 106462. https://doi.org/10.1016/j.cemconres.2021.106462
Mailyan, L. R., Beskopylny, A. N., Meskhi, B., Stel'makh, S. A., Shcherban, E. M., & Ananova, O. (2021). Optimization of composition and technological factors for the lightweight fiber-reinforced concrete production on a combined aggregate with an increased coefficient of structural quality. *Applied Sciences*. https://doi.org/10.3390/app11167284
Meng, L., Zhang, C., Wei, J., Li, L., Liu, J., Wang, S., & Ding, Y. (2023). Mechanical properties and microstructure of ultra-high strength concrete with lightweight aggregate. *Case Studies in Construction Materials, 18*, Article e01745. https://doi.org/10.1016/j.cscm.2022.e01745
Meng, W., & Khayat, K. (2017). Effects of saturated lightweight sand content on key characteristics of ultra-high-performance concrete. *Cement and Concrete Research, 101*, 46–54. https://doi.org/10.1016/j.cemconres.2017.08.018
Mo, K. H., Yap, S. P., Alengaram, U. J., Jumaat, M. Z., & Bu, C. H. (2014). Impact resistance of hybrid fibre-reinforced oil palm shell concrete. *Construction and Building Materials, 50*, 499–507. https://doi.org/10.1016/j.conbuildmat.2013.10.016
Mohamed, A. M., Tayeh, B. A., Abu Aisheh, Y. I., & Salih, M. N. A. (2023). Exploring the performance of steel fiber reinforced lightweight concrete: A case study review. *Case Studies in Construction Materials, 18*, Article e01968. https://doi.org/10.1016/j.cscm.2023.e01968
Mohammed, B. S., Anwar Hossain, K. M., Eng Swee, J. T., Wong, G., & Abdullahi, M. (2012). Properties of crumb rubber hollow concrete block. *Journal of Cleaner Production, 23*, 57–67. https://doi.org/10.1016/j.jclepro.2011.10.035
Nazari, A., & Riahi, S. (2011). The role of SiO2 nanoparticles and ground granulated blast furnace slag admixtures on physical, thermal and mechanical properties of self compacting concrete. *Materials Science & Engineering A, 528*, 2149–2157. https://doi.org/10.1016/j.msea.2010.11.064
Neithalath, N., Weiss, J., & Olek, J. (2006). Characterizing enhanced porosity concrete using electrical impedance to predict acoustic and hydraulic performance. *Cement and Concrete Research, 36*, 2074–2085. https://doi.org/10.1016/j.cemconres.2006.09.001
Nguyen, D. L., Thai, D. K., Nguyen, H. T. T., Tran, N. T., Phan, T. D., & Kim, D. J. (2023). Mechanical behaviors and their correlations of ultra-high-performance fiber-reinforced concretes with various steel fiber types. *Structural Concrete, 24*, 1179–1200. https://doi.org/10.1002/suco.202100184
Phan, T. D., Nguyen, V. T., & Kim, D. J. (2025). Predicting dynamic increase factors for post-cracking tensile strength of fiber-reinforced cement composites using novel hybrid machine learning models. *Construction and Building Materials, 489*, Article 142332. https://doi.org/10.1016/j.conbuildmat.2025.142332
Poongodi, K., & Murthi, P. (2020). Impact strength enhancement of banana fibre reinforced lightweight self-compacting concrete. *Materials Today: Proceedings, 27*, 1203–1209. https://doi.org/10.1016/j.matpr.2020.02.108
Raj, A., Sathyan, D., & Mini, K. M. (2019). Physical and functional characteristics of foam concrete: A review. *Construction and Building Materials, 221*, 787–799. https://doi.org/10.1016/j.conbuildmat.2019.06.052
Ramamurthy, K., Nambiar, E. K. K., & Ranjani, G. I. S. (2009). A classification of studies on properties of foam concrete. *Cement and Concrete Composites, 31*, 388–396. https://doi.org/10.1016/j.cemconcomp.2009.04.006
Rashad, A. M. (2018). Lightweight expanded clay aggregate as a building material – An overview. *Construction and Building Materials, 170*, 757–775. https://doi.org/10.1016/j.conbuildmat.2018.03.009
Rico, S., Farshidpour, R., & Tehrani, F. M. (2017). State-of-the-art report on fiber-reinforced lightweight aggregate concrete masonry. *Advances in Civil Engineering*. https://doi.org/10.1155/2017/8078346
Şahmaran, M., Lachemi, M., Hossain, K. M. A., & Li, V. C. (2009). Internal curing of engineered cementitious composites for prevention of early age autogenous shrinkage cracking. *Cement and Concrete Research, 39*, 893–901. https://doi.org/10.1016/j.cemconres.2009.07.006
Shafigh, P., Hafez, M. A., Che Muda, Z., Beddu, S., Zakaria, A., & Almkahal, Z. (2022). Influence of different ambient temperatures on the thermal properties of fiber-reinforced structural lightweight aggregate concrete. *Buildings*. https://doi.org/10.3390/buildings12060771
Shafigh, P., Mahmud, H., & Jumaat, M. Z. (2011). Effect of steel fiber on the mechanical properties of oil palm shell lightweight concrete. *Materials & Design, 32*, 3926–3932. https://doi.org/10.1016/j.matdes.2011.02.055
Shcherban', E. M., Stel'makh, S. A., Beskopylny, A., Mailyan, L. R., Meskhi, B., & Varavka, V. (2021). Nanomodification of lightweight fiber reinforced concrete with micro silica and its influence on the constructive quality coefficient. *Materials*. https://doi.org/10.3390/ma14237347
Shen, P., Lu, J. X., Lu, L., He, Y., Wang, F., & Hu, S. (2021). An alternative method for performance improvement of ultra-high performance concrete by internal curing: Role of physicochemical properties of saturated lightweight fine aggregate. *Construction and Building Materials, 312*, Article 125373. https://doi.org/10.1016/j.conbuildmat.2021.125373
Shen, P., Lu, J. X., Zheng, H., Lu, L., Wang, F., He, Y., & Hu, S. (2020a). Expansive ultra-high performance concrete for concrete-filled steel tube applications. *Cement and Concrete Composites, 114*, Article 103813. https://doi.org/10.1016/j.cemconcomp.2020.103813
Shen, P., Lu, L., Wang, F., He, Y., Hu, S., Lu, J., & Zheng, H. (2020b). Water desorption characteristics of saturated lightweight fine aggregate in ultra-high performance concrete. *Cement & Concrete Composites, 106*, Article 103456. https://doi.org/10.1016/j.cemconcomp.2019.103456
Shi, J., Lu, Y., Zhu, R., Liu, Y., Zhang, Y., & Lv, Q. (2024). Experimental evaluation of fracture toughness of basalt macro fiber reinforced high performance lightweight aggregate concrete. *Construction and Building Materials, 411*, Article 134638. https://doi.org/10.1016/j.conbuildmat.2023.134638
Simões, T., Octávio, C., Valença, J., Costa, H., Dias-da-Costa, D., & Júlio, E. (2017). Influence of concrete strength and steel fibre geometry on the fibre/matrix interface. *Composites Part B: Engineering, 122*, 156–164. https://doi.org/10.1016/j.compositesb.2017.04.010
Sjah, J., Chandra, J., Rastandi, J. I., & Arijoeni, E. (2018). The effect of usage of crushed polypropylene plastic waste in mechanical properties of concrete. *International Journal of Civil Engineering and Technology, 9*, 1495–1505.
Sohel, K. M. A., Al-Jabri, K., Zhang, M. H., & Liew, J. Y. R. (2018). Flexural fatigue behavior of ultra-lightweight cement composite and high strength lightweight aggregate concrete. *Construction and Building Materials, 173*, 90–100. https://doi.org/10.1016/j.conbuildmat.2018.03.276

Sukontasukkul, P. (2009). Use of crumb rubber to improve thermal and sound properties of pre-cast concrete panel. *Construction and Building Materials, 23*, 1084–1092. https://doi.org/10.1016/j.conbuildmat.2008.05.021
Swamy, R. N., et al. (1982). Workability of SFR lightweight aggregate concrete. *Internatioanl Journal of Cement Composites Lightweight Concretes, 4*, 103–109.
Tajra, F., Abd Elrahman, M., Lehmann, C., & Stephan, D. (2019). Properties of lightweight concrete made with core-shell structured lightweight aggregate. *Construction and Building Materials, 205*, 39–51. https://doi.org/10.1016/j.conbuildmat.2019.01.194
Talebi, H. R., Kayan, B. A., Asadi, I., & Hassan, Z. F. B. A. (2020). Investigation of thermal properties of normal weight concrete for different strength classes. *Journal of Environmental Treatement Techniques, 8*(3), 908–914.
Tang, C. W. (2020). Residual mechanical properties of fiber-reinforced lightweight aggregate concrete after exposure to elevated temperatures. *Applied Sciences*. https://doi.org/10.3390/app10103519
Tiwari, V., Shukla, A., & Bose, A. (2004). Acoustic properties of cenosphere reinforced cement and asphalt concrete. *Applied Acoustics, 65*, 263–275. https://doi.org/10.1016/j.apacoust.2003.09.002
Trabelsi, A., & Kammoun, Z. (2020). Mechanical properties and impact resistance of a high-strength lightweight concrete incorporating prickly pear fibres. *Construction and Building Materials, 262*, Article 119972. https://doi.org/10.1016/j.conbuildmat.2020.119972
Wang, H. T., & Wang, L. C. (2013). Experimental study on static and dynamic mechanical properties of steel fiber reinforced lightweight aggregate concrete. *Construction and Building Materials, 38*, 1146–1151. https://doi.org/10.1016/j.conbuildmat.2012.09.016
Wang, J. Y., Chia, K. S., Liew, J. Y. R., & Zhang, M. H. (2013). Flexural performance of fiber-reinforced ultra lightweight cement composites with low fiber content. *Cement and Concrete Composites, 43*, 39–47. https://doi.org/10.1016/j.cemconcomp.2013.06.006
Wang, X., Yu, R., Song, Q., Shui, Z., Liu, Z., Wu, S., & Hou, D. (2019). Optimized design of ultra-high performance concrete (UHPC) with a high wet packing density. *Cement and Concrete Research, 126*, Article 105921. https://doi.org/10.1016/j.cemconres.2019.105921
Wei, H., Wu, T., & Yang, X. (2020). Properties of lightweight aggregate concrete reinforced with carbon and/or polypropylene fibers. *Materials*. https://doi.org/10.3390/ma13030640
Wu, J., Ding, Q., Liu, Y., Mei, J., Zhang, G. (2021). Mixture design, preparation and properties of lightweight ultra-high performance concrete (LUHPC). 20: 3–10. https://doi.org/10.21838/uhpc.9642.
Wu, T., Yang, X., Wei, H., & Liu, X. (2019). Mechanical properties and microstructure of lightweight aggregate concrete with and without fibers. *Construction and Building Materials, 199*, 526–539. https://doi.org/10.1016/j.conbuildmat.2018.12.037
Xiang, Z., Zhou, J., & Niu, J. (2022). Compressive behavior of CFRP-confined steel fiber-reinforced self-compacting lightweight aggregate concrete in square columns. *Journal of Building Engineering, 59*, Article 105118. https://doi.org/10.1016/j.jobe.2022.105118
Xie, Y., Zhou, Q., Long, G., Chaktrimongkol, P., Shi, Y., & Umar, H. A. (2022). Experimental investigation on mechanical property and microstructure of ultra-high-performance concrete with ceramsite sand. *Structural Concrete, 23*, 2391–2404. https://doi.org/10.1002/suco.202100156
Xu, B., Toutanji, H. A., & Gilbert, J. (2010). Impact resistance of poly(vinyl alcohol) fiber reinforced high-performance organic aggregate cementitious material. *Cement and Concrete Research, 40*, 347–351. https://doi.org/10.1016/j.cemconres.2009.09.006
Yahaghi, J., Muda, Z. C., & Beddu, S. B. (2016). Impact resistance of oil palm shells concrete reinforced with polypropylene fibre. *Construction and Building Materials, 123*, 394–403. https://doi.org/10.1016/j.conbuildmat.2016.07.026
Yap, S. P., Alengaram, U. J., Jumaat, M. Z., & Khaw, K. R. (2016). Torsional and cracking characteristics of steel fiber-reinforced oil palm shell lightweight concrete. *Journal of Composite Materials, 50*, 115–128. https://doi.org/10.1177/0021998315571431
Ye, Y., Liu, J., Zhang, Z., Wang, Z., & Peng, Q. (2020). Experimental study of High-Strength Steel Fiber Lightweight Aggregate Concrete on mechanical properties and toughness index. *Advances in Materials Science and Engineering*. https://doi.org/10.1155/2020/5915034
Yew, M. K., Bin Mahmud, H., Ang, B. C., & Yew, M. C. (2015). Influence of different types of polypropylene fibre on the mechanical properties of high-strength oil palm shell lightweight concrete. *Construction and Building Materials, 90*, 36–43. https://doi.org/10.1016/j.conbuildmat.2015.04.024
Yu, K., Zhu, H., Hou, M., & Li, V. C. (2021). Self-healing of PE-fiber reinforced lightweight high-strength engineered cementitious composite. *Cement and Concrete Composites, 123*, Article 104209. https://doi.org/10.1016/j.cemconcomp.2021.104209
Yu, Q. L., Spiesz, P., & Brouwers, H. J. H. (2015). Ultra-lightweight concrete: Conceptual design and performance evaluation. *Cement and Concrete Composites, 61*, 18–28. https://doi.org/10.1016/j.cemconcomp.2015.04.012
Yun, T. S., Jeong, Y. J., & Youm, K. S. (2014). Effect of surrogate aggregates on the thermal conductivity of concrete at ambient and elevated temperatures. *The Scientific World Journal*. https://doi.org/10.1155/2014/939632
Zeng, Y., Sun, P., Tang, A., & Zhou, X. (2020). Shear performance of lightweight aggregate concrete with and without chopped fiber reinforced. *Construction and Building Materials, 263*, Article 120187. https://doi.org/10.1016/j.conbuildmat.2020.120187
Zhang, D., Tan, K. H., Dasari, A., & Weng, Y. (2020). Effect of natural fibers on thermal spalling resistance of ultra-high performance concrete. *Cement and Concrete Composites, 109*, Article 103512. https://doi.org/10.1016/j.cemconcomp.2020.103512
Zhang, G., Zhang, W., Li, Y., Chen, H., Ge, J., Pan, Y., & Hou, D. (2024). The effect of curing regimes on the hydration products of lightweight ultra-high performance concrete: From experiments to MD simulations. *Construction and Building Materials, 412*, Article 134865. https://doi.org/10.1016/j.conbuildmat.2024.134865
Zhang, Y., Feng, P., Zhang, S., Zhao, W., Yan, Z., Zhu, H., & Ju, J. W. (2025). Experimental study on the fracture behavior of a novel multi-scale fiber reinforced ultra-high performance concrete with hollow microspheres after high temperatures. *Engineering Fracture Mechanics*. https://doi.org/10.1016/j.engfracmech.2025.110979
Zhao, M., Zhang, B., Shang, P., Fu, Y., Zhang, X., & Zhao, S. (2019). Complete stress-strain curves of self-compacting steel fiber reinforced expanded-shale lightweight concrete under uniaxial compression. *Materials*. https://doi.org/10.3390/ma12182979
Zhao, S., Li, C., Zhao, M., & Zhang, X. (2016). Experimental study on autogenous and drying shrinkage of steel fiber reinforced lightweight-aggregate concrete. *Advances in Materials Science and Engineering*. https://doi.org/10.1155/2016/2589383
Zheng, R., Gao, G., Yu, Z., Wang, B., Zhou, A., Song, Q., & Bao, J. (2025). Dynamic mechanical properties of fiber-reinforced lightweight aggregate concrete exposed to high temperature. *Journal of Building Engineering, 103*, Article 112161. https://doi.org/10.1016/j.jobe.2025.112161
Zheng, X., Ji, T., Easa, S. M., Zhang, B., & Jiang, Z. (2019). Tensile basic creep behavior of lightweight aggregate concrete reinforced with steel fiber. *Construction and Building Materials, 200*, 356–367. https://doi.org/10.1016/j.conbuildmat.2018.12.138
Zou, S., Lu, J. X., Xiao, J., Duan, Z., Kong Chau, C., Lung Sham, M., & Sun Poon, C. (2023). Development and characteristics of novel high-strength lightweight core-shell aggregate. *Construction and Building Materials, 393*, Article 132080. https://doi.org/10.1016/j.conbuildmat.2023.132080

Publisher's Note

Su Sung Jo PhD Candidate in Sejong University

Tan Duy Phan PhD Candidate in Hanyang University.

Do Hyung Lee Professor in PaiChai University.

Sang Yeop Chung Associate professor in Yonsei University.

Dong Joo Kim Professor in Hanyang University.